



HAL
open science

Forearc seafloor unconformities and geology: insight from 3D seismic geomorphology analysis, Peru

Gérôme Calvès, Constance Auguy, Léopold de Lavaissière, Stéphane Brusset,
Ysabel Calderon, Patrice Baby

► **To cite this version:**

Gérôme Calvès, Constance Auguy, Léopold de Lavaissière, Stéphane Brusset, Ysabel Calderon, et al.. Forearc seafloor unconformities and geology: insight from 3D seismic geomorphology analysis, Peru. *Geochemistry, Geophysics, Geosystems*, 2017, <10.1002/2017GC007036>. <hal-01569621>

HAL Id: hal-01569621

<https://hal.science/hal-01569621v1>

Submitted on 27 Jul 2017






HAL is a multi-disciplinary open access archive for the deposit and dissemination of scientific research documents, whether they are published or not. The documents may come from teaching and research institutions in France or abroad, or from public or private research centers.

L'archive ouverte pluridisciplinaire **HAL**, est destinée au dépôt et à la diffusion de documents scientifiques de niveau recherche, publiés ou non, émanant des établissements d'enseignement et de recherche français ou étrangers, des laboratoires publics ou privés.



Distributed under a Creative Commons CC0 1.0 - Universal - International License

Forearc seafloor unconformities and geology: insight from 3D seismic geomorphology analysis, Peru

Gérôme Calvès¹  (orcid.org/0000-0003-3829-131X), Constance Auguy¹ (orcid.org/0000-0003-1060-4425), Léopold de Lavaissière¹  (orcid.org/0000-0002-3063-3103), Stéphane Brusset¹  (orcid.org/0000-0002-7880-4514), Ysabel Calderon^{1, 2}  (orcid.org/0000-0003-1060-4425), Patrice Baby^{1, 2, 3}  (orcid.org/0000-0001-6142-5174).

¹Université Toulouse 3, Paul Sabatier, OMP-GET, 14 avenue Edouard Belin, 31400-F, Toulouse, France.

²PeruPetro, Lima, Peru.

³ Institut de recherche pour le développement (IRD).

Corresponding author: Gérôme Calvès (gerome.calves@get.omp.eu)

Key Points:

- Unconformities at forearc seafloor are associated with erosive power of oceanic bottom currents and/or wave action.
- The observed unconformity surfaces cover 18–100% of the seafloor at the studied sites.
- Estimates of sedimentation rate and paleo-productivity in such regions are assessed with regard to unconformities and hiatuses.

This article has been accepted for publication and undergone full peer review but has not been through the copyediting, typesetting, pagination and proofreading process which may lead to differences between this version and the Version of Record. Please cite this article as doi: 10.1002/2017GC007036

© 2017 American Geophysical Union

Received: May 26, 2017; Revised: Jun 29, 2017; Accepted: Jun 29, 2017

20 **Abstract**

21 New 3D seismic data collected over 4870 km² in the 3°45'–12°30'S Peruvian segment of the East
22 Pacific subduction system image seafloor erosional surfaces that can be mapped across the
23 forearc basins. Forearc basins experience various stresses, from their base where basal tectonic
24 erosion acts to the seafloor which is influenced by aerial, shallow and deep water currents driven
25 by waves or thermohaline oceanic currents. Previously there has been little interest in stresses on
26 the upper layer and there is a lack of documentation of unconformities and the erosive processes
27 in certain bathymetric domains in forearc basins. We address this with the study of examples
28 sourced from 3D seismic reflection surveys of the seafloor offshore Peru. Unconformities occur
29 in two distinctive bathymetric domains associated with the continental shelf and the upper slope
30 of the margin. Identification and characterization of unconformity surfaces yield estimates of the
31 amount of erosion at the modern seafloor that range from 18 to 100%. Regional physical
32 oceanography allows us to calibrate potential candidates for these two distinctive domains. The
33 first control on erosion is the dynamics of deep to intermediate oceanic currents related to the
34 Humboldt-Peru Chile water masses, while the second is wave action in the shallower erosional
35 surfaces. This study illustrates the unseen landscape of the forearc basins of South America and
36 helps to highlight the importance of erosive surficial processes in subduction landscapes.

37 **Keywords:**

38 Forearc basin, seafloor, 3D seismic reflection, seismic geomorphology, discontinuities,
39 unconformities, erosion, Humboldt Peru-Chile current, Peru.

40 **1 Introduction**

41 Marginal systems offshore continents have for a long period of time been documented as
42 depositional systems with limited attention to the unconformities observed on the continental
43 shelf and their erosion-related processes [*Blackwelder*, 1909; *Cotton*, 1918; *Hay*, 2015; *Miall*,

44 2016; *Vail et al.*, 1980]. Another important aspect is the dynamics of erosion of fine grained
45 sediments that has not yet been fully understood [e.g., *McCave*, 1984]. The context of strong
46 erosion from on- to offshore has been rarely studied and quantified. As an example, the offshore
47 domain of the rising orogenic island of Taiwan has been well documented, although constraints
48 on submarine erosion and its forcing mechanisms have not been clearly understood [*Ramsey et*
49 *al.*, 2006]. Along the Pacific margin of North and South America, coastal erosion has been
50 mainly investigated at rocky shores where paleo-shorelines emerge or drowned, as a result of
51 various uplift events [e.g., *Shepard and Grant*, 1947; *Clift and Hartley*, 2007; *Saillard, et al.*,
52 2009; *Jara-Muñoz et al.*, 2017]. Various cyclic stresses affect the margin in these places. The
53 two most important are: waves sourced by the strong westerly winds in the Southern Ocean
54 [*Beccario*, earth.nullschool.net; *López, et al.*, 2015] and along-margin oceanic currents such as
55 the Peru-Chile (Humboldt) Currents [*Chaigneau et al.*, 2013] (Figure 1). Sediment archives at
56 the seafloor from 3 to 18°S are characteristic of current-dominated regimes [*Reinhardt, et al.*,
57 2002] with ongoing phosphorite formation, tide-topography interaction and resultant non-linear
58 internal waves [*Erdem et al.*, 2016]. Mooring experiments documented current speeds of up to
59 20 cm/s in the upper 200 m of the continental shelf of Peru from 5°S to 15°30'S [*Brockmann, et*
60 *al.*, 1980].

61 Continental shelves offshore South America are an important region for the study of
62 resources and the interactions of atmospheric and oceanographic processes in solid Earth
63 sciences. Peruvian forearc basins (Figure 1) [*Dickinson*, 1995; *Noda*, 2016] have been imaged
64 using sub-bottom profilers and multibeam echosounders [*Reinhardt, et al.*, 2002] during research
65 cruises and sampled by dredges, shallow piston cores, the Ocean Drilling Program [e.g., *Suess et*
66 *al.*, 1988], and by oil and gas exploration wells. Most of the academic geoscientific work on

67 Peruvian forearc basins has been performed offshore in the deep water domain (>200m water
68 depth). This has allowed understanding of the distal part of the margin and its relationship with
69 the subducting plate, in the area of the trench to the upper slope. Structure and infill have been
70 studied using 2D seismic reflection surveys [e.g., *Thornburg and Kulm, 1981; Kulm et al., 1982;*
71 *Moore and Taylor, 1988*]. The structural framework of the margin and forearc basins worldwide
72 has been divided into two types, with one related to subduction accretion and the second to basal
73 tectonic erosion [e.g., *Clift et al., 2003; Clift and Vannucchi, 2004*] (Figure 2). Many subsurface
74 discontinuities have been studied in order to document subsidence and basal erosion of
75 accretionary margins [e.g., *Scholl et al., 1980; von Huene and Lallemand, 1990*]. The oldest
76 basal unconformity identified in forearc basins is related to the interface between the structurally
77 active or passive basement of the overriding plate within the context of the subduction zone
78 (Figure 2). The subsequent unconformities within the forearc stratigraphy then depend on the
79 vertical movements and the source of sediments (volcaniclastic, siliciclastics, and in-situ
80 produced carbonates) and record erosional events and hiatuses depending on the rates of
81 sedimentation. Unconformities at the seafloor are one of the least recognized and documented
82 surfaces in the evolution of forearc basins.

83 Seismic technology has advanced in the third dimension [*Cartwright and Huuse, 2005*],
84 thus allowing sedimentary basins to be assessed with an unprecedented level of detail. Three-
85 dimensional seismic data can be used to study sub-seafloor geology in detail, such as that
86 observed by high-resolution bathymetry [*Bulat, 2005; Grant and Schreiber, 1990*]. Seafloor
87 features offer a window to the deeper subsurface of a given sedimentary basin and so resolve
88 Earth surface processes identified from preserved features [*Bourgeois et al., 1988; Sosson et al.,*
89 *1994; Collier et al., 2006; Gupta et al., 2007; Huuse, 2011; Mitchell et al., 2013*]. The seafloor

90 bathymetry, combined with deep penetration seismic reflection surveys, is commonly used to
91 document the mechanical and tectonic behavior of accretionary margins [e.g., *Beaudry and*
92 *Moore*, 1981; *Gulick, et al.*, 2010; *McNeill and Henstock*; 2014; *Frederik, et al.*, 2015], but is
93 rarely used to constrain external forces acting on the top of the margin slope.

94 The Peru offshore domain represents an area of 900,000 km² of which 82,000 km² are
95 associated with the continental shelf. The offshore domain, its water column conditions and
96 seafloor habitat of a major interest to those concerned with fish populations in the Peruvian
97 upwelling ecosystem [*Gallardo* 1977; *Arntz et al.*, 1991]. The importance of bathymetric
98 information has been shown along the Peru margin not only for Earth sciences, but also for life
99 sciences. Limited knowledge on shallow bathymetric environments south of 10°S, i.e. the
100 morphology of the continental shelf, is key to models of water column biological processes and
101 prevents an understanding of how sediments (Fe) contribute to the development of
102 phytoplankton [*Echevin et al.*, 2008]. The only seafloor erosion documented on 2D seismic
103 reflection grid offshore Peru and potentially related to bottom currents has been done by
104 *Ballestros et al.* (1998) for water depth greater than 2000 m in the Yaquina and Lima
105 sedimentary basins [*Clift et al.*, 2003].

106 Our aim is to document the present-day seafloor bathymetry, acoustic properties and
107 geology in the near subsurface using 3D seismic reflection data from four sedimentary basins off
108 the coast of Peru. From North to South these basins are named: Tumbes, Talara, Salaverry, and
109 Pisco (Figures 1 and 2). Our specific interest is in the identification of constructive and
110 destructive surfaces that record the seafloor of these forearc basins.

111 **2 Data and methods**

112 Our seismic data set covers most of these forearc basins, covering a bathymetric range of 20 to
113 2040 m, in the offshore Peru area (Figures 1 and 3). The data used for the current study are 3D
114 multi-channel, post-stack, time-migrated reflection seismic data. They were acquired within
115 exploration areas offshore Peru and are named based on these hydrocarbon exploration license
116 numerations. The seismic data displayed in this study are zero phase and have the Society of
117 Exploration Geophysicists (SEG) normal polarity, i.e. black peak indicating an increase in
118 acoustic impedance. We use seismic attributes to enhance sedimentary to structural features that
119 occur from the seafloor to the subsurface. The seismic attributes are extracted from the two-way
120 time horizon mapped within the 3D seismic reflection data. We use a constant velocity (1500
121 m/s) for depth conversion of the seafloor from time to depth domain. The details of each seismic
122 data set and seafloor surfaces are summarized in Table 1. The 3D seismic data in this study have
123 been interpreted using standard seismic stratigraphic techniques [*Mitchum et al., 1977; Vail et*
124 *al., 1977*] and seismic geomorphology principles [*Posamentier et al., 2007*] based on reflection
125 terminations and seismic facies reflection characteristics. The seafloor reflection can show
126 concordance (no termination) or truncation (erosional or structural). The seafloor reflection and
127 surrounding reflections are interpreted as a sequence boundary [*Mitchum et al., 1977*]. The
128 vertical resolution of the shallow section of the six seismic cubes range is 8 to 12 m. With this
129 vertical resolution, the near-seafloor 3D seismic provides stratigraphical and geomorphological
130 insights into the architecture that would normally be sub-seismic scale in the deeper subsurface
131 [*Steffens et al., 2004*].

132 Oceanographic data (temperature, salinity, wave observations) are sourced from National
133 Oceanic and Atmospheric Administration (NOAA) world ocean database (WOD13, Station
134 7538849(C)) [*Boyer et al., 2013*] and the NOAA National Data Buoy Center (Station 32012 -

135 Woods Hole Stratus Wave Station, data from 2007 to 2015) (<http://www.ndbc.noaa.gov>). We
136 have converted the wave frequency to wavelength using the deep-water gravity equation [*Lamb*,
137 1994]: $\lambda = g/(2\pi f^2)$, where g is gravitational acceleration and f is the wave frequency measured in
138 Hz. The depth of penetration of wave action (i.e. capacity to entrain sediment at the mudline
139 interface) is defined as one half of its wavelength [*Reading and Collinson*, 1996].

140 **3. Results**

141 3.1 Seafloor bathymetry and morphology

142 Observed features at the seafloor from 3°45'S to 12°30'S span two main morphological domains:
143 the shelf and the upper slope (Figures 1 and 3, Table 1). In the Tumbes Basin (Z1 and Z38;
144 Figures 3a and 3b), the seafloor dips from NE to SW over a depth range from about 20 m to
145 1380 m within the area surveyed by 3D seismic data. The mean slope is gentle and ranges from
146 2.6 to 3.6°. Local increases in slope are related to structural features (see below). Along the
147 margin the Talara Basin (Figures 1, 3c and 3d) is covered by two 3D seismic surveys. The
148 seafloor dips from E to W, with a depth range from ~190 m to 2040 m, within the area surveyed
149 by 3D seismic data. The mean slope is moderate and ranges from ~6 to 10°. In the northern area
150 (Z34A; Figure 3c) the upper slope shows a steep margin deepening to a smooth flat seafloor
151 surface. In the southern area (Z34E; Figure 3d) the shelf extends as a low angle surface that
152 marks the shallower part of the upper slope that evolves to an incised deep and steep topographic
153 depression that runs along an east to west axis. These two depressions are related to two deep
154 water canyons named La Bocana and Paita (Figure 3d). These two canyons have not yet been
155 surveyed. They are named from the nearest towns along the coast and are located north of the
156 Chiclayo Canyon (7°S) described by *Sosson et al.* [1994]. Further south in the Salaverry Basin
157 (Z35; Figure 3e), the seafloor dips from ENE to WSW over a depth range from ~110 m to ~200

158 m within the area surveyed by 3D seismic data. The mean slope is low, with a value of 1.75° .
159 The last surveyed area is within the Pisco Basin (Z33; Figure 3f). The seafloor dips from NE to
160 SW with a depth range from ~100 m to ~320 m within the area surveyed by 3D seismic data.
161 The mean slope is low with a value of 1° . Features observed at the seafloor are summarized in
162 Table 2. We first describe unconformities at the seafloor of each sedimentary basin/data set from
163 North to South along the Peruvian offshore domain, after which we document other preserved
164 features.

165 3.2 Seafloor unconformities

166 3.2.1 Tumbes Basin seafloor unconformities

167 Observed seafloor unconformities in the Tumbes Basin seismic reflection data (Figure 4a) are
168 related to five different configurations. The first configuration is associated with toplap
169 termination with a high angle dipping into subsurface sequences structured by faults (Figure 4b).
170 This is well marked by seismic amplitude changes and abrupt changes over the discontinuity
171 towards the north of the study area. These structures occur in the shallower domains of the study
172 area. The unconformities cover extensive areas from 10 km² to over 100 km² (Figure 4c). The
173 second configuration is related to lower angle toplap terminations that are prolonged by
174 continuous reflections that extend seaward (Figure 4d). The third is also associated with low-
175 angle toplap terminations that in this area are prolonged over short distances and closed loop by
176 other toplap terminations and an undulating high amplitude erosional truncation (Figure 4d).
177 These mark mounded structures over areas of 30 to >40 km² located in the SW of the study area
178 (Figure 4c). The mounded structures have a long axis orientated NNE-SSW, with a length >2
179 km, an amplitude of 20 m and a wavelength of 0.4–1.0 km. These structures are restricted to
180 water depths >200 m. We interpret them as contourite drifts. These features are observed in area

181 Z38 (Figure 5a). The seafloor seismic reflection amplitude map shows important variations, from
182 continuous high amplitude to localized linear to rounded low amplitude areas (Figure 5b). The
183 fourth configuration is associated with high angle toplap terminations that are associated with
184 flat top erosional truncations (Figure 5c). One example is the Banco Peru that is located in the
185 western part of the Tumbes Basin. These structures occur over local highs that show a different
186 level of flatness. They show low to moderate amplitude values compared to the surrounding
187 concordant higher amplitude seafloor reflections (Figure 5b). These erosional unconformities
188 extend over areas >10 km². They are expressed in a wide range of bathymetric domains (Figures
189 5c and 5d). The fifth and last configuration of erosional unconformities at the seafloor in the
190 Tumbes Basin is characterized by toplap high angle, with faulted underlying sequences that are
191 rounded and positive mounds overlapped by surrounding continuous, younger seismic sequences
192 (Figures 5c and 5d). They are related to tectonically uplifted structures that have been previously
193 eroded under other conditions. Between all these various types of unconformities, 44% of the
194 seafloor surface of the Tumbes Basin is subject to erosion (Table 2).

195 3.2.2 Talara Basin seafloor unconformities

196 The observed unconformities at the seafloor seismic reflections in the northern part of the Talara
197 Basin (Z34A; Figure 6a) are related to seven different configurations. The seafloor amplitude
198 shows a range of values, with low values associated with steep slopes and higher amplitude
199 values related to concordant reflections at the seafloor (Figure 6b). The similarity attribute shows
200 extensive areas of highly continuous reflection (Figure 6c). The first configuration of
201 unconformities is associated with toplap termination with low angle reflections that are bounded
202 in their opposite direction by other toplap terminations that also mark erosional truncations
203 (Figure 6d). The unconformity ranges from 15 to 36 m in height (Figure 6d). This configuration

204 is interpreted as the flank of a detached drift contourite, and its steep, eroded slopes. A second
205 configuration is associated with toplap terminations that are associated with steep relief of a
206 minimum 80, ranging up to 150 m that marks a scarp or an escarpment (Figures 6b and 6d). This
207 scarp is associated with removal of material downslope in relation to mass wasting processes.
208 The third configuration is associated with low similarity and low reflectivity acoustic basement
209 outcropping at the seafloor. This type is localized at the transition from the high angle slope of
210 the margin and the lower basin fills (Figures 6c and 6d). The fourth and fifth show toplap
211 terminations and erosional unconformities related to incisions, such as channels or canyons in the
212 slope. These channels or canyons (Figures 6a and 7a) incise the seafloor from 40 m up to 360 m
213 respectively along their walls that have lower amplitude reflection strength compared to basal
214 infill and inter-canyon deposits (Figures 6b and 7b). Two deep-water canyons are observed in the
215 southern part of the Talara Basin. These canyons are named Paita and La Bocana. The sixth
216 configuration is associated with low angle seaward toplap termination and erosional truncation in
217 the upper slope over a bathymetric range of 1400 to ~400 m (Figure 7a). These are strictly
218 associated with erosive surfaces and do not contain depositional features. The seventh and last
219 configuration observed at the Talara Basin seafloor marks an extensive erosional unconformity
220 that shows high angle reflections associated with faults and tilted blocks (Figures 7c and 7d). The
221 surficial average unconformity covers 36% of the area within the 3D seismic survey (Table 2).

222 3.2.3 Salaverry Basin seafloor unconformities

223 The observed seafloor unconformity in the Salaverry Basin (Z35; Figure 8a) is related to one
224 configuration over two different types of sedimentary structures. The complete surface is
225 associated with toplap terminations of various angles that mark the subsurface geology. The
226 overall basin is truncated at the seafloor and highlights the sedimentary basin infill. Faults are

227 expressed at the seafloor in the western part of the survey (Figure 8b). The eastern seismic
228 reflections and sequences are tilted with an overall synclinal structure (Figures 8c and 8d).
229 Truncated seismic structures outcropping at the seafloor are related to canyons infills or
230 prograding clinoform sets (Figures 8b and 8d). The surficial unconformity covers 100% of the
231 area surveyed by 3D seismic data (Table 2). This is the highest surficial erosion observed along
232 the entire Peru Margin.

233 3.2.4 Pisco Basin seafloor unconformities

234 The observed unconformity at the seafloor seismic reflection in the Pisco Basin (Z33; Figure 9a)
235 is related to one configuration of sedimentary structures. The seafloor reflection surface has
236 various amplitude values (Figure 9b) and associated with concordant, toplap termination
237 reflections with low angle and erosional truncation (Figure 9c). The erosional truncation cuts a
238 progradational sequence (Figures 9b and d) that is incised by linear to convergent seaward
239 channels. This unconformity occurs over a bathymetric range of 125–160 m. The surficial
240 unconformity covers 29% of the surveyed area by 3D seismic (Table 2). This marks the highest
241 preserved depositional area within the regions studied offshore Peru.

242 3.3 seafloor fluid flow features

243 Within the surveyed area, a number of non-sedimentary features have been identified at the
244 seafloor reflection. Localized small-scale seafloor depressions in the Tumbes and Talara Basins
245 are pockmarks (Figures 5 and 6), related to fluid escape through underlying vertical gas
246 chimneys. These are spatially located above reversed-polarity reflections (relative to the
247 seafloor) known as bottom-simulating reflections (BSRs) that are commonly associated with free
248 gas trapped beneath a layer of methane hydrate-bearing sediment. They are related to the
249 occurrence of a velocity and impedance contrast related to the hydrate-bearing layers.

250 **4. Discussion**

251 4.1 Morphological features of unconformities

252 With observations of seafloor unconformities from different latitudes and depths along the
253 Peruvian forearc basins, we identify potential processes related to these features. A synthetic
254 diagram illustrates the occurrence of unconformities (Figure 10). Unconformities are observed in
255 the two investigated domains, the shelf and upper slope. In the northern part of the Peruvian
256 margin, these two domains express various types of erosive surfaces. As far south as 5°S in the
257 Talara Basin (Figure 1) unconformities occur at two different levels/water depths along the upper
258 slope: one shallow (~200–300m) and one deeper (~900–1100 m) (Figure 10). South of 5°S the
259 unconformities are observed at the shelf/upper slope transition as well as deeper water ~300 m.
260 *Krissek et al.* [1980] and *Reiners and Suess* [1983] documented the absence of sedimentation at
261 the shelf break north of 10°30'S and south of 15°S. A water depth of 200–300 m corresponds to
262 the transition from the upper to intermediate water masses. Unconformities occur south of 5°S
263 (Figure 10), as well depicted in the Salaverry Basin (8°S) where the seafloor is recognized as
264 being a continuous unconformity (Figure 8).

265 4.2 Seafloor and physical oceanography interaction

266 The primary surficial water mass movements within the study area are the action of oceanic
267 waves sourced from far field activity in the Southern Ocean as well as waves generated by local
268 southerly winds in the Eastern Pacific Ocean bordered by the Andes (Figure 1). The wave action
269 is expressed by a wave base depth of penetration with two modes, the first peak at 55 m and the
270 second at ~150 m water depth (Figure 10) as recorded by buoys offshore Peru (Station 32012 -
271 Woods Hole Stratus Wave Station, data from 2007 to 2015) (<http://www.ndbc.noaa.gov>). The
272 frequency and depth of action associated with these waves are surficial and decrease drastically
273 as the seafloor depth increases.

274 The secondary water mass movements are associated with the Humboldt-Peru-Chile
275 Currents (Figure 1) [e.g., *Chaigneau et al.*, 2013; *Czeschel et al.*, 2015]. These currents have the
276 strength to displace and remove significant amounts of sediment and generate unconformities at
277 the seafloor (Figure 10). In some places, deep water currents might induce a strong shearing
278 momentum at the seafloor where they interfere. Such configuration is observed along the Peru
279 margin when the Peru-Chile Undercurrent (PCUC) and Chile-Peru Deep Coastal Current
280 (CPDCC) occur together (Figure 1). The prime example in this study is in the Salaverry area
281 (Figure 11) where we have observed the most complete unconformity. Where only deep currents
282 erode the seafloor, the magnitude of the unconformity decreases such as that seen in the Pisco
283 Basin. This place has a counter part with an important coastal upwelling and high production rate
284 of sediments [*Krissek et al.*, 1980] that might balance the unconformity expression.

285 In the northern part of the Peruvian margin in the Tumbes and Talara Basins, we identify
286 important erosion surfaces that are expressed in the water depth range of the surface currents,
287 such as the Ecuador-Peru Coastal Current (EPCC), and the associated subsurface currents, e.g.,
288 the Equatorial Undercurrent (EUC) (Figures 10 and 11) [*Chaigneau et al.*, 2013]. The complex
289 seafloor geometry of bathymetric highs in the Tumbes Basin might cause the strength of the
290 currents to increase and accelerate at these localities, focusing the erosion (Figure 5). The
291 presence of moats and contourite drifts in bathymetric domains over 600 m water depth (Figures
292 5, 6 and 7) is diagnostic of a potential strong active bottom current associated with the
293 Northward-spreading Antarctic Intermediate Water (AAIW) and the Pacific Central Water
294 (PCW) [*Tsuchiya and Talley*, 1998]. In the Tumbes Basin, Banco Peru (Figure 1) is an isolated
295 structural high that has a flat top platform in water depths of ~100 m (Figure 5) and is subject to
296 wave action that can be as deep as 300 m offshore Peru (Figure 10). Further east, towards the

297 shore, these same waves can surge and stress the seafloor; this is highlighted by the strong
298 erosional unconformity surface that is observed from 200 m up to 26 m, at the shallowest limit of
299 the surveyed area (Figure 4). The complex interaction between wave action and oceanic currents
300 plays an important role in the near-coastal circulation and upwelling system of Peru [e.g., *Pietri*
301 *et al.*, 2014].

302 These unconformities might not be related to a single period of stress but instead are a
303 combination spanning long periods of time, as suggested by sedimentary archives offshore Peru
304 preserved in a bathymetric range of 90 to 1300 m and latitudes from 3 to 18°S [*Erdem et al.*,
305 2016]. Along the Chilean margin at 40°S strong shelf currents sweep all fine-grained material
306 [*Hebbeln et al.*, 2001]. Sediments are channelized directly into the deep sea trench through the
307 numerous canyons [*Moberly et al.*, 1982; *Hagen et al.*, 1994]. Further south in Chile the same
308 observations and processes are shaping the seafloor of the offshore prism [*Bernhardt et al.*, 2015
309 and 2016]. We have direct evidence of this on the slope of Talara Basin, with lobes at the mouth
310 of deep-water canyons (Figure 6). Deep-water sedimentation in this area is associated with
311 contourite drifts (this study) and suggests possible contributions from oceanic currents as
312 conveyors of particles to the deep-water sediments along the margin [*Muñoz et al.*, 2004].

313 An important goal remains to identify the action and erosive power of deep water
314 currents downslope in the least studied water depth range of the upper slope. This is not
315 investigated or quantified by physical oceanography studies along the upper slope of the Peru
316 margin >1000 m.

317 4.3 Seafloor basin dynamics: depositional dynamics

318 The identification of unconformities at the edge of significant packages of sediment, such as
319 canyons and/or contourite drifts in the upper slope of the Peru margin show the importance of

320 lateral sedimentation along such margins outside the continental shelf (Figures 5, 6, 7). The
321 continental shelf has been the focus of numerous studies over the past decades in relation with
322 upwelling [*Suess, 1980; Shipboard Scientific Party, 1988*] and accretionary/forearc basin genesis
323 [e.g., *Thornburg and Kulm, 1981; Ballesteros et al., 1988; Clift et al., 2003*]. Careful estimates of
324 deposition and erosion in such sedimentary basins could have an important role in calibrating
325 sediment budgets and flux [*Clift and Vannucchi, 2004; Stern, 2011*], and/or syntectonic
326 sedimentation history [*Simpson, 2010; Vannucchi, et al., 2016*] in a subducting geodynamic
327 framework. Regional estimates of recent sedimentation rates underline these limitations in such
328 settings [*Muñoz et al., 2004*]. In the Lima and Pisco Basins (Figure 1), Ocean Drilling Program
329 Sites 679, 680, 681, 686 and 687 documented important discontinuities at the seafloor or in the
330 subsurface, with numerous hiatuses spanning the last 11 m.y. [e.g., *Shipboard Scientific Party,*
331 *1988; Ballesteros et al., 1988*]. Buried unconformities in accretionary prisms are used to infer the
332 evolution of the subduction factory. The occurrence of regional unconformities must be
333 evaluated not only in the context of downslope mass movement or tectonic displacement. The
334 role of external processes such as climate processes (trade winds, wave action and strength)
335 and/or oceanic movements might play an important role in shaping these margins [*Koenitz et al.,*
336 *2008*].

337 4.4 Seafloor unconformities and fluid flow indicators,
338 Despite the identification of strong unconformity surfaces, the presence of fluid flow features at
339 the seafloor marks the signature of the fluids migrating updip within the forearc structure. Fluids
340 are acknowledged to play an important role in the evolution of collisional margins and their
341 related basins [*Moore and Vrolijk, 1992*]. Within the studied area we have identified sediment
342 remobilization features, such as pockmarks [*van Rensbergen et al., 2003*]. These are spatially

343 related to vertical discontinuities that are at the apex of faults of various types and in some areas
344 with the occurrence of potential gas hydrates as marked by bottom-simulating reflectors (BSR)
345 (Figures 5 and 6) [Auguy *et al.*, 2017]. Shallow subsurface hydrological and hydrate systems
346 within forearc basins offshore Peru have been identified [e.g., Kukowski and Pecher, 1999; von
347 Huene and Pecher, 1999]. Unconformities in the Tumbes Basin associated with outcropping
348 faulted structural highs are direct open conduits for fluid escape from the lower forearc and
349 accreted structures in these margins. The role of the bottom currents in erosion/deposition as well
350 as associated temperature variations has not yet been investigated. This could lead to a new
351 evaluation of the buried hydrates systems and their past evolution.

352 4.5 Seafloor unconformities and paleoenvironment record,
353 Our study underlines the importance of site location if a continuous or at least minimally
354 reworked sequence is required for paleoenvironmental analysis. Further south, mud lenses
355 located under the stress of the Peru-Chile Undercurrent (PCUC) [Salvatteci *et al.*, 2014] show
356 that laminae preservation at the regional scale is related to oxygen minimum zone intensity
357 changes as well as variations in the strength of bottom currents. Erosion and winnowing of
358 sediments by bottom currents could lead to uncertainties when computing absolute sedimentation
359 rate [Krissek *et al.*, 1980] and thus to budgets of biomass production and paleo-productivity
360 estimates. Flushed sediments from onshore rivers caused by extreme runoff associated with
361 strong El Niño events are dispersed over hundreds of kilometers along the shelf by the Peru
362 Current and countercurrent [Scheidegger and Krissek, 1982; Rein *et al.*, 2005]. De Vries and
363 Percy [1982] studied fish debris and associated sediment along the margin and noted that these
364 have been sorted during or after deposition.

365 **5. Conclusions**

366 Based on the analysis of seafloor reflection and interpretation of our 3D seismic reflection data,
367 we have mapped unconformities within the forearc basins of the Peru margin. From these results
368 we infer the following conclusions:

369 -1: Mapping of 3D seismic intervals in the near-seafloor interval provides new insights to
370 continental shelf and upper slope depositional processes and architectures. This could be
371 extended to other provinces around the Pacific margins in subduction settings.

372 -2: The seismic geomorphology and reflection termination study of the seafloor shows important
373 unconformity surfaces of various types over a wide range of water depths and latitudinal range.
374 These have been framed within the present knowledge of the physical oceanography and are
375 associated with bottom currents related to the Humboldt Peru-Chile Current as well as the wave
376 dynamics of the eastern Pacific Ocean. These two movements of oceanic water mark important
377 positive spatial and vertical correlations with the observed unconformity surfaces at the seafloor.

378 -3: Typology of seafloor unconformity surfaces can be subdivided into structural or sedimentary
379 origin with or without oceanic currents or wave action interaction. The role of the oceanic
380 physical stress to the seafloor is of prime importance in shaping the margin and its evolution.

381 -4: Many research topics from solid Earth, paleoenvironmental changes to biological sciences
382 have yet failed to integrate these important unconformities and hiatuses as biases in their work.
383 Care needs to be taken in future research when working in such settings.

384 **Acknowledgments**

385 This research project was conducted under the IRD-PERUPETRO S.A agreement. Seismic
386 reflection data are archived at the PeruPetro Data Bank (<http://www.perupetro.com.pe>). Other
387 sources are appropriately specified and cited. dGB Earth Sciences - OpendTect and IHS -
388 Kingdom are thanked for their Software University Grants, which have allowed this work to take

389 place. Thanks to Alexis Chaigneau (IRD, LEGOS, Toulouse), Peter D. Clift (Louisiana State
 390 University), Samuel Toucanne (IFREMER, LGS, Plouzané) and Mads Huuse (University of
 391 Manchester) for valuable discussions. The editor Thorsten Becker, G.F. Moore, (University of
 392 Hawaii) and an anonymous reviewer are thanked for their constructive comments.

393

394 **Tables**

Sedimentary basin	Dataset / seismic cube	Latitude	Bathymetry		Survey area km ²	Peak frequency Hz	Tuning thickness - vertical resolution m	Slope mean (degree)	Domain
			min (m)	max (m)					
Tumbes	Z1	3°45' S	24	411	1300	40	10	3,6	Shelf and upper slope
	Z38	4°15' S	99	1380	1620	43	9	2,6	Shelf and upper slope
Talara	Z34A	4°20' S	946	1895	194	47	8	5,95	Upper slope
	Z34E	5°S	196	2040	215	35	11	10	Shelf and upper slope
Salaverry	Z35	8°S	112	202	880	35	11	1,75	Shelf
Pisco	Z33	12°3' 0'S	108	323	663	32	12	1	Shelf and upper slope

395

396 **Table 1:** Geographical and morphological properties of the seafloor for the four sedimentary
 397 basins within the 3D seismic reflection data used for this study.

Sedimentary basin	Dataset / seismic cube	Feature/shape				Interpretation			Unconformity % (minimum/mean/maximum)
		linear	rounded	mounds	flat top high	Structural	Sedimentary	Fluid flow	

Tumbes	Z1	x	x	x		faults / uplifted structure s	erosional unconformitie s, contourite drift,	pockmar ks	26/44/68
	Z38	x	x	x	x	faults / uplifted structure s	erosional unconformitie s, contourite drift, moat	pockmar ks	
Talara	Z34A	x	x	x	x	faults	erosional unconformitie s, head scarp of mass wasting, contourite drift, channel, lobe	pockmar ks	18/36/53
	Z34E	x	x	x		fault	erosional unconformitie s, canyons, contourite drift	not identified	
Salaverry	Z35	x	x		x	fault	erosional unconformitie s, prograding canyon infill, canyon edges	not identified	100
Pisco	Z33	x			x	not identifie d	erosional unconformitie s, channels, wave cut platform	not identified	29

398

399 **Table 2:** Morphological and seismic properties of the various features observed within the 3D
400 seismic data volumes used for this study, and their interpretation.

401 **Figures**

402 **Figure 1:** Peru Continental Margin main forearc basins imaged with 3D seismic reflection data
403 and investigated (surveys: Z1, Z38, Z34A&E, Z35). (a) Arrows indicate general flow directions
404 of surface currents (SEC: South Equatorial Current; EPCC: Ecuador-Peru Coastal Current; PCC:
405 Peru Coastal Current; POC: Peru Oceanic Current) and subsurface currents (EUC: Equatorial

406 Undercurrent; pSSCC: primary (northern branch) Southern Subsurface Countercurrent; sSSCC:
407 sSSCC: secondary (southern branch) Southern Subsurface Countercurrent; PCCC: Peru-Chile
408 Countercurrent; CPDCC: Chile-Peru Deep Coastal Current; PCUC: Peru-Chile Undercurrent)
409 [e.g., *Chaigneau et al.*, 2013] along the Peru-Ecuador margin. (b) Offshore Peru wave rose
410 diagram of an average year in terms of significant wave height (Hs) [*Lopez et al.*, 2015].

411 **Figure 2:** Peruvian forearc basins and studied areas framed in the diagrams showing the features
412 common to the two basic types of active margin: (a) accretionary and (b) erosive [adapted from
413 Clift and Vannuchi, 2004]. Study areas and data set are located by the black rectangle above their
414 respective type of active margin.

415 **Figure 3:** Bathymetric perspective views of the seafloor over the 3D seismic data used for this
416 study in four different forearc basins offshore Peru (a. and b.: Tumbes; c. and d.: Talara; e.:
417 Salaverry; f.: Pisco). The reader is referred to Table 1 for bathymetric ranges for each area.

418 **Figure 4:** Seafloor geomorphological (bathymetry: a) and seismic reflection properties
419 (amplitude: b and semblance: c) within Tumbes Z1 area. Seismic cross section (d) uninterpreted
420 and interpreted from Tumbes Z1 area. Concordant, toplap terminations and erosional truncations
421 are associated with the seafloor seismic reflection. Faults and pockmarks are outcropping at the
422 seafloor. An uplifted and eroded structure is outcropping in the northern part of the study area
423 and is onlapped by recent reflection packages marked by a disconformity. The cross-hatch
424 surfaces represent the labelled erosional truncation surfaces at the seafloor.

425 **Figure 5:** Seafloor geomorphological (bathymetry: a) and seismic reflection properties
426 (amplitude: b and similarity: c) within Tumbes Z38 area. Seismic cross section (d) uninterpreted

427 and interpreted from Tumbes Z38 area. Concordant, toplap terminations and erosional
428 truncations are associated with the seafloor seismic reflection. Two sets of faults outcrop at the
429 seafloor with orientation WNW-ESE and SW-NE respectively. Two types of mounded structures
430 are observed, the first associated with a flat topped geometry and erosional truncations, and a
431 second with smaller mounded elongated features related to contourite drifts. Pockmarks are
432 observed to the SW of the study area, they are rooted from vertical discontinuities associated
433 with gas chimneys. An uplifted erode structure is outcropping at the seafloor to the NE. The
434 Banco Peru marks a prominent flat top structure that shoals in the NW part of the Tumbes Basin.
435 The cross-hatch surfaces represent the labelled erosional truncation surfaces at the seafloor.

436 **Figure 6:** Seafloor geomorphological (bathymetry: a) and seismic reflection properties
437 (amplitude: b and similarity: c) within Talara Z34A area. Seismic cross section (d) uninterpreted
438 and interpreted from Talara Z34A area. Concordant, toplap terminations and erosional
439 truncations are associated with the seafloor seismic reflection. Channels and lobes are sourced
440 from the slope to pounded basins in the northern part of the study area. Between these,
441 pockmarks are outcropping. These are associated to vertical discontinuities related to gas
442 chimneys. Isolated mounds in the slope are associated with detached contourite drifts. Their
443 edges are marked by erosional truncation. A negative seismic reflection crosscutting the
444 surrounding seismic reflection corresponds to the “bottom-simulating reflection” (BSR). This
445 marks the occurrence of potential gas hydrates and free gas in the subsurface. The cross-hatch
446 surfaces represent the labelled erosional truncation surfaces at the seafloor.

447 **Figure 7:** Seafloor geomorphological (bathymetry: a) and seismic reflection properties
448 (amplitude: b and similarity: c) within Talara Z34E area. Seismic cross section (d) uninterpreted

449 and interpreted from Talara Z34E area. Concordant, toplap terminations and erosional
450 truncations are associated with the seafloor seismic reflection. Canyon walls are associated with
451 toplap terminations and erosional truncations. The upper slope is composed of depositional
452 features associated with contourite drift in the intercanyon area and erosional truncations updip.
453 The shelf shows an important erosional truncation with outcropping faults of the overlying
454 rotated faulted blocks. The cross-hatch surfaces represent the labelled erosional truncation
455 surfaces at the seafloor.

456 **Figure 8:** Seafloor geomorphological (bathymetry: a) and seismic reflection properties
457 (amplitude: b and similarity: c) within Salaverry Z35 area. Seismic cross section (d)
458 uninterpreted and interpreted from Salaverry Z35 area. Toplap terminations and erosional
459 truncations are associated with the seafloor seismic reflection. Various geometries are truncated,
460 of which progradational sequences or canyons infills. The outcropping seismic sequences shows
461 an older to younger stratigraphic age landward. The cross-hatch surfaces represent the labelled
462 erosional truncation surfaces at the seafloor.

463 **Figure 9:** Seafloor geomorphological (bathymetry: a) and seismic reflection properties
464 (amplitude: b and similarity: c) within Pisco Z33 area. Seismic cross section (d) uninterpreted
465 and interpreted from Pisco Z33 area. Concordant, toplap terminations and erosional truncations
466 are associated with the seafloor seismic reflection. An erosional truncation cuts a progradational
467 sequence that is incised by linear to convergent seaward channel. The cross-hatch surfaces
468 represent the labeled erosional truncation surfaces at the seafloor.

469 **Figure 10:** Synthesis of the depth of unconformities and oceanographic properties along the
470 Peruvian margin. CTD station 7538849(C) and oceanographic data are from NOAA world ocean

471 database WOD13. Water masses names are sourced from *Chaigneau et al.* [2013] (see Figure 1
472 and caption) and references within. Along shore integrated transport corresponds to the mean
473 cross-shore section at 7°S–13°S between the coast and 200 km offshore.

474 **Figure 11:** Perspective view of the Peruvian margin and strength of erosion by oceanic processes
475 (see Table 2). Arrows indicate general flow directions of surface currents (EPCC: Ecuador-Peru
476 Coastal Current; PCC: Peru Coastal Current); and subsurface currents (EUC: Equatorial
477 Undercurrent; pSSCC: primary (northern branch); CPDCC: Chile-Peru Deep Coastal Current;
478 PCUC: Peru-Chile Undercurrent) [e.g., *Chaigneau et al.*, 2013].

479 **References**

- 480 Arntz, W. E., J Tarazona, V Gallardo, L. A. Flores, and H Salzwedel (1991), Benthos
481 communities in oxygen deficient shelf and upper slope areas of the Peruvian and Chilean Pacific
482 coast, and changes caused by El Niño, *Geological Society, London, Special Publications*, 58,
483 131–154, doi:10.1144/GSL.SP.1991.058.01.10
- 484 Auguy, C., G. Calvès, Y. Calderon, and S. Brusset (2017), Seismic evidence of gas hydrates,
485 multiple BSRs and fluid flow offshore Tumbes Basin - Peru, *Marine Geophysical Research*, 1–
486 15, doi:10.1007/s11001-017-9319-2
- 487 Ballesteros, M.W., G.F. Moore, B. Taylor, and S. Ruppert (1988), Seismic stratigraphic
488 framework of the Lima and Yaquina forearc basins, Peru. In: Suess, E., von Huene, R., et al.,
489 Proc. ODP, Init. Repts., 112: College Station, TX (Ocean Drilling Program), 77–90.
490 doi:10.2973/odp.proc.ir.112.105.1988
- 491 Beaudry, D. and G. F. Moore (1981), Seismic-stratigraphic framework of the forearc basin off
492 central Sumatra, Sunda Arc, *Earth and Planetary Science Letters*, 54(1), 17–28,
493 doi:10.1016/0012-821X(81)90065-0.
- 494 Bernhardt, A., D. Melnick, J. Jara-Muñoz, B. Argandoña, J. González, and M. R. Strecker
495 (2015), Controls on submarine canyon activity during sea-level highstands: The Biobío canyon
496 system offshore Chile, *Geosphere*, 11 (4), 1226–1255, doi: 10.1130/GES01063.1
- 497 Bernhardt, A., D. Hebbeln, M. Regenberg, A. Lückge, and M. R. Strecker (2016), Shelfal
498 sediment transport by an undercurrent forces turbidity-current activity during high sea level
499 along the Chile continental margin, *Geology*, 44, 295–298, doi:10.1130/G37594.1

- 500 Blackwelder, E. (1909), The Valuation of Unconformities, *The Journal of Geology*, 17(3), 289–
501 299, Retrieved from <http://www.jstor.org/stable/30068167>
- 502 Bourgois, J., G. Pautot, W. Bandy, T. Boinet, P. Chotin, P. Huchon, B. Mercier de Lepinay, F.
503 Monge, J. Monlau, B. Pelletier, M. Sosson, and R. von Huene (1988), Seabeam and seismic
504 reflection imaging of the tectonic regime of the Andean continental margin off Peru (4°S to
505 10°S), *Earth and Planetary Science Letters*, 87(1–2), 111–126, doi:10.1016/0012-
506 821X(88)90068-4
- 507 Boyer, T.P., J. I. Antonov, O. K. Baranova, C. Coleman, H. E. Garcia, A. Grodsky, D. R.
508 Johnson, R. A. Locarnini, A. V. Mishonov, T.D. O'Brien, C.R. Paver, J.R. Reagan, D. Seidov, I.
509 V. Smolyar, and M. M. Zweng (2013), World Ocean Database 2013, NOAA Atlas NESDIS 72,
510 S. Levitus, Ed., A. Mishonov, Technical Ed.; Silver Spring, MD, 209 pp., doi:
511 10.7289/V5NZ85MT
- 512 Brockmann, C., E. Fahrback, A. Huyer, and R.L. Smith (1980), The poleward undercurrent
513 along the Peru coast: 5 to 15°S, *Deep Sea Research Part A. Oceanographic Research Papers*,
514 27(10), 847–856, doi:10.1016/0198-0149(80)90048-5.
- 515 Bulat J. (2005), Some considerations on the interpretation of seabed images based on
516 commercial 3D seismic in the Faroe-Shetland Channel, *Basin Research*, 17, 21–42,
517 doi:10.1111/j.1365-2117.2005.00253.x
- 518 Cartwright J. and M. Huuse (2005), 3D seismic technology: the geological ‘Hubble’, *Basin*
519 *Research*, 17(1), 1–20, doi: 10.1111/j.1365-2117.2005.00252.x
- 520 Chaigneau, A., N. Dominguez, G. Eldin, L. Vasquez, R. Flores, C. Grados, and V. Echevin
521 (2013), Near-coastal circulation in the Northern Humboldt Current System from shipboard
522 ADCP data, *J. Geophys. Res. Oceans*, 118, 5251–5266, doi:10.1002/jgrc.20328.
- 523 Clift, P.D., and A.J. Hartley (2007), Slow rates of subduction erosion along the Andean margin
524 and reduced global crustal recycling, *Geology*, 35(6), 503–506, doi: 10.1130/G23584A.1
- 525 Clift, P. D., I. Pecher, N. Kukowski, and A. Hampel (2003), Tectonic erosion of the Peruvian
526 forearc, Lima Basin, by subduction and Nazca Ridge collision, *Tectonics*, 22, 1023,
527 doi:10.1029/2002TC001386, 3.
- 528 Clift, P., and P. Vannucchi (2004), Controls on tectonic accretion versus erosion in subduction
529 zones: Implications for the origin and recycling of the continental crust, *Reviews of Geophysics*,
530 v. 42, p. RG2001, doi:10.1029/2003RG000127
- 531 Collier, J. S., S. Gupta, G. Potter, and A. Palmer-Felgate (2006), Using bathymetry to identify
532 basin inversion structures on the English Channel shelf, *Geology*, 34(12), 1001–1004,
533 doi:10.1130/G22714A.1

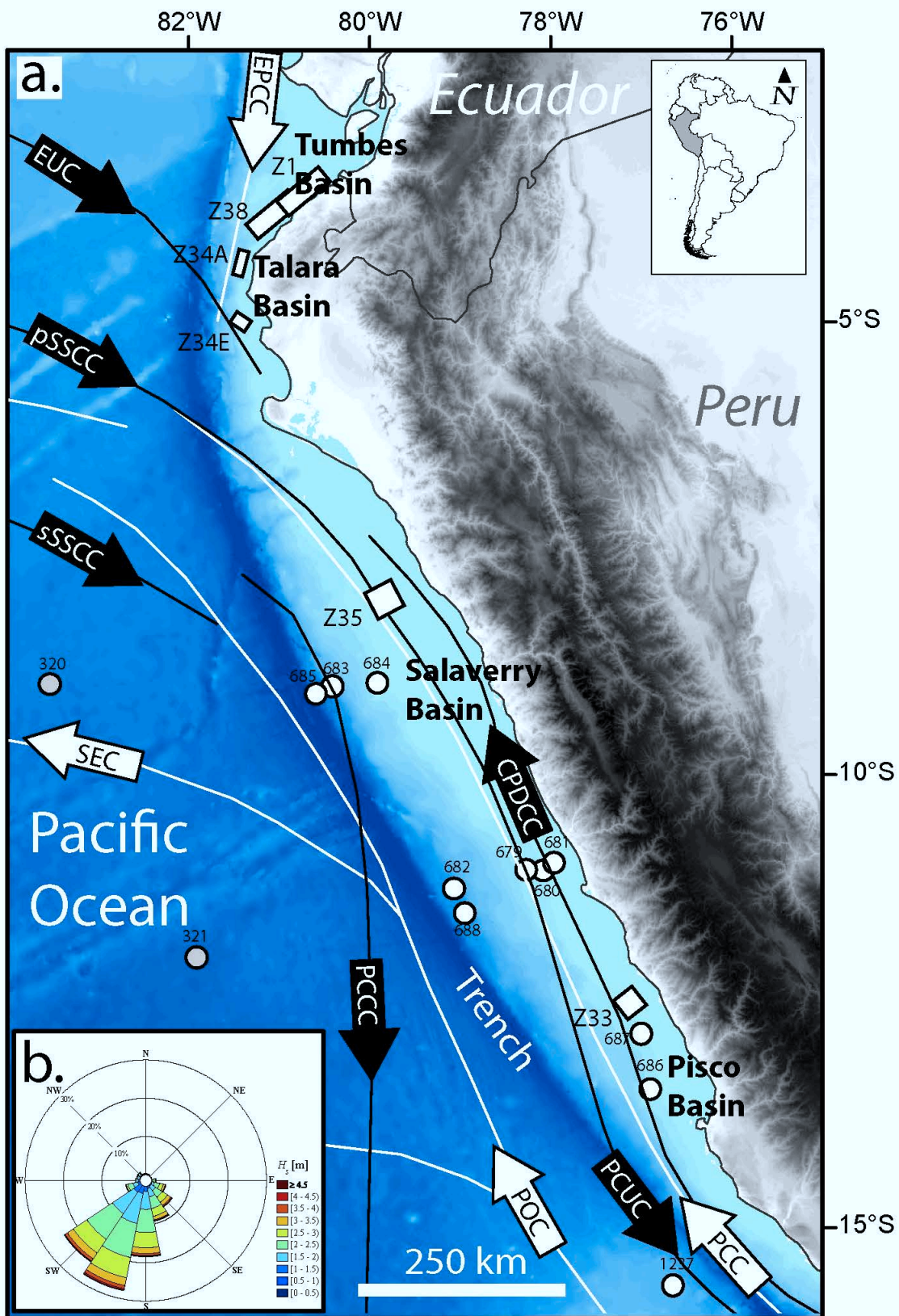
- 534 Cotton, C. (1918), Conditions of deposition on the continental shelf and slope, *The Journal of*
535 *Geology*, 26(2), 135–160. Retrieved from <http://www.jstor.org/stable/30080728>
- 536 De Vries, T. J., and W. G. Percy (1982), Fish debris in sediments of the upwelling zone off
537 central Peru: a late Quaternary record, *Deep Sea Research Part A. Oceanographic Research*
538 *Papers*, 29(1), 87–109, doi:10.1016/0198-0149(82)90063-2.
- 539 Dickinson, W.R. (1995), Forearc basins. In: *Tectonics of Sedimentary basins* (Ed. by C.J. Busby
540 and R.V. Ingersoll) p. 221–261, Blackwell Scientific Publications, Oxford
- 541 Echevin, V., O. Aumont, J. Ledesma, and G. Flores (2008), The seasonal cycle of surface
542 chlorophyll in the Peruvian upwelling system: A modelling study, *Progress in Oceanography*, 79
543 (2–4), 167–176, doi:10.1016/j.pocean.2008.10.026.
- 544 Erdem, Z., J. Schönfeld, N. Glock, M. Dengler, T. Mosch, S. Sommer, J. Elger, and A.
545 Eisenhauer (2016), Peruvian sediments as recorders of an evolving hiatus for the last 22
546 thousand years, *Quaternary Science Reviews*, 137, 1–14, doi: 10.1016/j.quascirev.2016.01.029.
- 547 Frederik, M. C. G., S. P. S. Gulick, J. A. Austin Jr., N. L. B. Bangs, and Udrekx (2015), What 2-
548 D multichannel seismic and multibeam bathymetric data tell us about the North Sumatra wedge
549 structure and coseismic response, *Tectonics*, 34, 1910–1926, doi:10.1002/2014TC003614.
- 550 Gallardo, VA (1977), Large benthic microbial communities in sulphide biota under Peru-Chile
551 subsurface countercurrent, *Nature*, 268, 331–332. doi:10.1038/268331a0s
- 552 Grant, J. A., and R. Schreiber (1990), Modern swathe sounding and sub-bottom profiling
553 technology for research applications: The Atlas Hydrosweep and Parasound Systems, *Marine*
554 *Geophysical Researches*, 12(1), 9–19, doi:10.1007/978-94-009-0615-0_2
- 555 Gulick, S.P.S., N.L.B. Bangs, G.F. Moore, J. Ashi, K.M. Martin, D.S. Sawyer, H.J. Tobin, S.
556 Kuramoto, and A. Taira (2010), Rapid forearc basin uplift and megasplay fault development
557 from 3D seismic images of Nankai Margin off Kii Peninsula, Japan, *Earth and Planetary*
558 *Science Letters*, 300(1–2), 55–62, doi:10.1016/j.epsl.2010.09.034.
- 559 Gupta, S., J. S. Collier, A. Palmer-Felgate and G. Potter (2007), Catastrophic flooding origin of
560 shelf valley systems in the English Channel, *Nature*, 448, 342–345. doi:10.1038/nature06018
- 561 Hagen, R.A., D. D. Bergersen, R. Moberly, and W. T. Coulbourn (1994), Morphology of a large
562 meandering submarine canyon system on the Peru-Chile forearc, *Marine Geology*, 119(1), 7–38,
563 doi:10.1016/0025-3227(94)90138-4.
- 564 Hay W.W. (2015), Erosion Hiatuses, *Encyclopedia of Marine Geosciences*, 1–5, doi:
565 10.1007/978-94-007-6644-0_57-5

- 566 Hebbeln D., M. Marchant, T. Freudenthal, and G. Wefer (2000), Surface sediment distribution
567 along the Chilean continental slope related to upwelling and productivity, *Marine Geology*,
568 164(3–4), 119–137, doi:10.1016/S0025-3227(99)00129-2.
- 569 Huuse, J. (2011), 3D seismic characterization of the Norwegian Channel Ice Stream: Spatio-
570 temporal evolution of a major cross-shelf trough through multiple glaciations, *Quaternary*
571 *International*, Volumes 279–280, 213, doi:10.1016/j.quaint.2012.08.420.
- 572 Jara-Muñoz, J., D. Melnick, P. Zambrano, A. Rietbrock, J. González, B. Argandoña and M. R.
573 Strecker (2017), Quantifying offshore fore-arc deformation and splay-fault slip using drowned
574 Pleistocene shorelines, Arauco Bay, Chile, *J. Geophys. Res. Solid Earth*, 122,
575 doi:10.1002/2016JB013339.
- 576 Koenitz, D., N. White, I. N. McCave, and R. Hobbs (2008), Internal structure of a contourite
577 drift generated by the Antarctic Circumpolar Current, *Geochem. Geophys. Geosyst.*, 9, Q06012,
578 doi:10.1029/2007GC001799.
- 579 Krissek, L. A., K. F. Scheidegger, and L. D. Kulm (1980), Surface sediments of the Peru-Chile
580 continental margin and the Nazca plate, *GSA Bulletin*, 91(6), 321–331; doi:10.1130/0016-
581 7606(1980)91<321:SSOTPC>2.0.CO;2
- 582 Kulm, L. D., T. M. Thornburg, H. J. Schraderand, and J. M. Resig (1982), Cenozoic structure,
583 stratigraphy and tectonics of the central Peru forearc, *Geological Society, London, Special*
584 *Publications*, 10(1), 151–169, doi:10.1144/GSL.SP.1982.010.01.10
- 585 Kulm, L. D., H. Schrader, J. M. Resig, T. M. Thornburg, A. Masias, and L. Johnson (1981), Late
586 Cenozoic carbonates on the Peru continental margin: Lithostratigraphy, biostratigraphy, and
587 tectonic history, *Geological Society of America Memoirs*, 154, 469–508, doi:10.1130/MEM154-
588 p469
- 589 Kukowski, N., and I. Pecher (1999), Thermo-hydraulics of the Peruvian accretionary complex at
590 12°S, *Journal of Geodynamics*, 27(3), 373–402, doi:10.1016/S0264-3707(98)00009-X.
- 591 Lamb H. (1994), *Hydrodynamics*: Cambridge, UK, Cambridge University Press, 768 p.
- 592 López, M., M. Veigas, and G. Iglesias (2015), On the wave energy resource of Peru, *Energy*
593 *Conversion and Management*, 90, 34–40, doi:10.1016/j.enconman.2014.11.012
- 594 McCave I. N. (1984), Erosion, transport and deposition of fine-grained marine sediments,
595 *Geological Society, London, Special Publications*, 15, 35–69,
596 doi:10.1144/GSL.SP.1984.015.01.03
- 597 McNeill, L. C., and T. J. Henstock (2014), Forearc structure and morphology along the Sumatra-
598 Andaman subduction zone, *Tectonics*, 33, 112–134, doi:10.1002/2012TC003264.

- 599 Miall, Andrew D. (2016), The valuation of unconformities, *Earth-Science Reviews*, 163, 22–71,
600 doi:10.1016/j.earscirev.2016.09.011
- 601 Mitchell, N. C., J. M. Huthnance, T. Schmitt and B. Todd (2013), Threshold of erosion of
602 submarine bedrock landscapes by tidal currents, *Earth Surface Processes and Landforms*, 38(6),
603 627–639, doi:10.1002/esp.3347
- 604 Mitchum, R. M., P. R. Vail, and J. B. Sangree (1977), Stratigraphic interpretation of seismic
605 reflection patterns in depositional sequences. part 6, in *Seismic Stratigraphy—Application to*
606 *Hydrocarbon Exploration*, 8th ed., edited by C. E. Payton, pp. 117–133, AAPG, Tulsa, Okla.
- 607 Moberly, R., G. L. Shepherd, and W. T. Coulbourn (1982), Forearc and other basins, continental
608 margin of northern and southern Peru and adjacent Ecuador and Chile, *Geological Society,*
609 *London, Special Publications*, 10(1), 171–189, doi:10.1144/GSL.SP.1982.010.01.11
- 610 Moore, G. F., and B. Taylor (1988), Structure of the Peru forearc from multichannel seismic
611 reflection data, *Proc. Ocean Drill. Program Initial Rep.*, 112, 71–76.
- 612 Moore, J. C., and P. Vrolijk (1992), Fluids in accretionary prisms, *Rev. Geophys.*, 30(2), 113–
613 135, doi:10.1029/92RG00201.
- 614 Muñoz, P., C.B. Lange, D. Gutiérrez, D. Hebbeln, M.A. Salamanca, L. Dezileau, J.L. Reyss, and
615 L.K. Benninger (2004), Recent sedimentation and mass accumulation rates based on ²¹⁰Pb
616 along the Peru–Chile continental margin, *Deep Sea Research Part II: Topical Studies in*
617 *Oceanography*, 51(20–21), 2523–2541, doi:10.1016/j.dsr2.2004.08.015.
- 618 Noda A. (2016), Forearc basins: Types, geometries, and relationships to subduction zone
619 dynamics, *GSA Bulletin*, 128(5–6), 879–895; doi:10.1130/B31345.1.
- 620 Pietri, A., V. Echevin, P. Testor, A. Chaigneau, L. Mortier, C. Grados, and A. Albert
621 (2014), Impact of a coastal-trapped wave on the near-coastal circulation of the Peru upwelling
622 system from glider data, *J. Geophys. Res. Oceans*, 119, 2109–2120, doi:10.1002/2013JC009270.
- 623 Posamentier, H. W., R. J. Davies, J. A. Cartwright, and L. Wood (2007). Seismic
624 geomorphology-an overview, *Geological Society, London, Special Publications*, 277(1), 1–14.
625 doi:10.1144/GSL.SP.2007.277.01.01
- 626 Ramsey, L. A., N. Hovius, D. Lague, and C.-S. Liu (2006), Topographic characteristics of the
627 submarine Taiwan orogen, *J. Geophys. Res.*, 111, F02009, doi:10.1029/2005JF000314.
- 628 Reading H.G., and J.D. Collinson (1996), Clastic coasts, in Reading H.G., ed., *Sedimentary*
629 *environments: Processes, facies and stratigraphy*: Oxford, UK, Blackwell Science, pp. 154–258.
- 630 Reimers, C.E., and E. Suess (1983), Spatial and temporal patterns of organic matter
631 accumulation on the Peru continental margin, in: *coastal Upwelling and its sedimentary record*

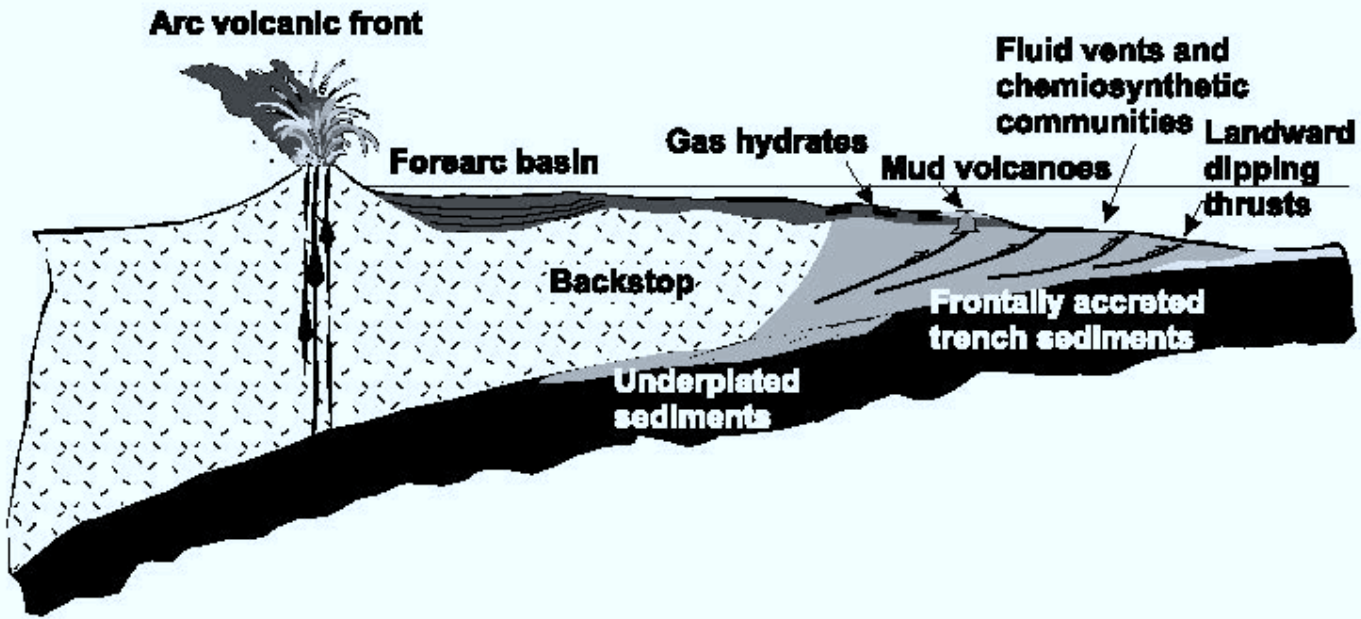
- 632 part B: Sedimentary Records of Ancient Coastal Upwelling. In: Thiede, J., Suess, E. (Eds.),
 633 NATO Conference Series IV: Mar. Sci., vol. 10b, pp. 311–346.
- 634 Rein, B., A. Lückge, L. Reinhardt, F. Sirocko, A. Wolf, and W.-C. Dullo (2005), El Niño
 635 variability off Peru during the last 20,000 years, *Paleoceanography*, 20, PA4003,
 636 doi:10.1029/2004PA001099.
- 637 Reinhardt, L., H.-R. Kudrass, A. Lückge, M. Wiedicke, J. Wunderlich, and G. Wendt (2002),
 638 High-resolution sediment echosounding off Peru: Late Quaternary depositional sequences and
 639 sedimentary structures of a current-dominated shelf, *Marine Geophysical Researches*, 23(4),
 640 335–351, doi:10.1023/A:1025781631558
- 641 Saillard, M., S.R. Hall, L. Audin, D.L. Farber, G. Hérail, J. Martinod, V. Regard, R.C. Finkel,
 642 and F. Bondoux (2009), Non-steady long-term uplift rates and Pleistocene marine terrace
 643 development along the Andean margin of Chile (31°S) inferred from ¹⁰Be dating, *Earth and*
 644 *Planetary Science Letters*, 277(1–2), 50–63, doi: 10.1016/j.epsl.2008.09.039
- 645 Salvattecchi, R., D. Field, A. Sifeddine, L. Ortlieb, V. Ferreira, T. Baumgartner, S. Caquineau, F.
 646 Velasco, J.-L.s Reyss, J.-A. Sanchez-Cabeza, and D. Gutierrez (2014), Cross-stratigraphies from
 647 a seismically active mud lens off Peru indicate horizontal extensions of laminae, missing
 648 sequences, and a need for multiple cores for high resolution records, *Marine Geology*, 357(1),
 649 72–89, doi:10.1016/j.margeo.2014.07.008.
- 650 Scheidegger, K. F., and L. A. Krissek (1982), Dispersal and deposition of eolian and fluvial
 651 sediments off Peru and northern Chile, *GSA Bulletin*, 93 (2) 150–162, doi:10.1130/0016-
 652 7606(1982)93<150:DADDOEA>2.0.CO;2
- 653 Scholl, D. W., R. von Huene, T. L. Vallier, and D. G. Howell (1980), Sedimentary masses and
 654 concepts about tectonic processes at underthrust ocean margins, *Geology*, 8 (12) 564–568; doi:
 655 10.1130/0091-7613(1980)8<564:SMACAT>2.0.CO;2
- 656 Shepard F. P. and U. S. Grant IV (1947), Wave erosion along the southern California Coast,
 657 *Geological Society of America Bulletin*, 58(10), 919–926, doi:10.1130/0016-
 658 7606(1947)58[919:WEATSC]2.0.CO;2
- 659 Shipboard Scientific Party, (1988), Introduction, objectives, and principal results, Leg 112, Peru
 660 continental margin, In: Suess, E., von Huene, R., et al., Proc. ODP, Init. Repts., 112: College
 661 Station, TX (Ocean Drilling Program), 5–23. doi:10.2973/odp.proc.ir.112.102.1988
- 662 Sosson, M., J. Bourgois, and B. Mercier de Lépinay (1994), SeaBeam and deep-sea submersible
 663 Nautilite surveys in the Chiclayo canyon off Peru (7°S): Subsidence and subduction-erosion of an
 664 Andean-type convergent margin since Pliocene times, *Marine Geology*, 118(3–4), 237–256,
 665 doi:10.1016/0025-3227(94)90086-8
- 666 Steffens, G. S., R. C. Shipp, B. E. Prather, J. A. Nott, J. L. Gibson and C. D. Winker (2004), The
 667 use of near-seafloor 3D seismic data in deepwater exploration and production (in 3D seismic

- 668 technology; application to the exploration of sedimentary basins, R. J. Davies, et al.), *Memoirs of*
669 *the Geological Society of London*, 29, 35–43, doi: 10.1144/GSL.MEM.2004.029.01.04.
- 670 Stern, C. R. (2011), Subduction erosion: Rates, mechanisms, and its role in arc magmatism and
671 the evolution of the continental crust and mantle, *Gondwana Research*, 20(2–3), 284–308,
672 doi:10.1016/j.gr.2011.03.006.
- 673 Suess, E. (1980), Particulate organic carbon flux in the oceans—surface productivity and oxygen
674 utilization, *Nature*, 288, 260–263, doi:10.1038/288260a0
- 675 Thornburg, T., and L. D. Kulm (1981), Sedimentary basins of the Peru continental margin:
676 Structure, stratigraphy, and Cenozoic tectonics from 6°S to 16°S latitude, *Geological Society of*
677 *America Memoirs*, 154, 393–422, doi:10.1130/MEM154-p393
- 678 Tsuchiya, M., and L. D. Talley (1998), A Pacific hydrographic section at 88°W: Water-property
679 distribution, *J. Geophys. Res.*, 103(C6), 12899–12918, doi:10.1029/97JC03415.
- 680 Vail, P. R., R. M. Mitchum, and S. Thompson (1977), Seismic stratigraphy and global changes
681 of sea-level. part 3: Relative changes of sea level from coastal onlap, in *Seismic Stratigraphy—*
682 *Applications to Hydrocarbon Exploration*, AAPG Mem., vol. 26, edited by C. E. Payton, pp. 63–
683 81, AAPG, Tulsa, Okla.
- 684 Vail, P. R., R. M. Mitchum, T. H. Shipley, R. T. Buffler, and D. H. Matthews (1980),
685 Unconformities of the North Atlantic [and Discussion], *Phil. Trans. R. Soc. Lond. A*, 294, 137–
686 155, doi:10.1098/rsta.1980.0021.
- 687 Van Rensbergen, P., R. R. Hillis, A. J. Maltman, and C. K. Morley (2003), Subsurface sediment
688 mobilization: introduction, *Geological Society, London, Special Publications*, 216, 1–8,
689 doi:10.1144/GSL.SP.2003.216.01.01.
- 690 Vannucchi, P., J. P. Morgan, E. A. Silver, and J. W. Kluesner (2016), Origin and dynamics of
691 depositional subduction margins, *Geochem. Geophys. Geosyst.*, 17, 1966–1974,
692 doi:10.1002/2016GC006259.
- 693 von Huene, R., and S. Lallemand (1990), Tectonic erosion along the Japan and Peru convergent
694 margins, *Geological Society of America Bulletin*, 102(6), 704–720, doi:10.1130/0016-
695 7606(1990)102<0704:TEATJA>2.3.CO;2
- 696 von Huene, R., and I. A. Pecher (1999), Vertical tectonics and the origins of BSRs along the Peru
697 margin, *Earth and Planetary Science Letters*, 166(1–2), 47–55, doi:10.1016/S0012-
698 821X(98)00274-X.
- 699 Witt C. and J. Bourgois (2010), Forearc basin formation in the tectonic wake of a collision-
700 driven, coastwise migrating crustal block: The example of the North Andean block and the
701 extensional Gulf of Guayaquil-Tumbes Basin (Ecuador-Peru border area), *Geological Society of*
702 *America Bulletin*, 122(1–2), 89–108, doi: 10.1130/B26386.1



a.

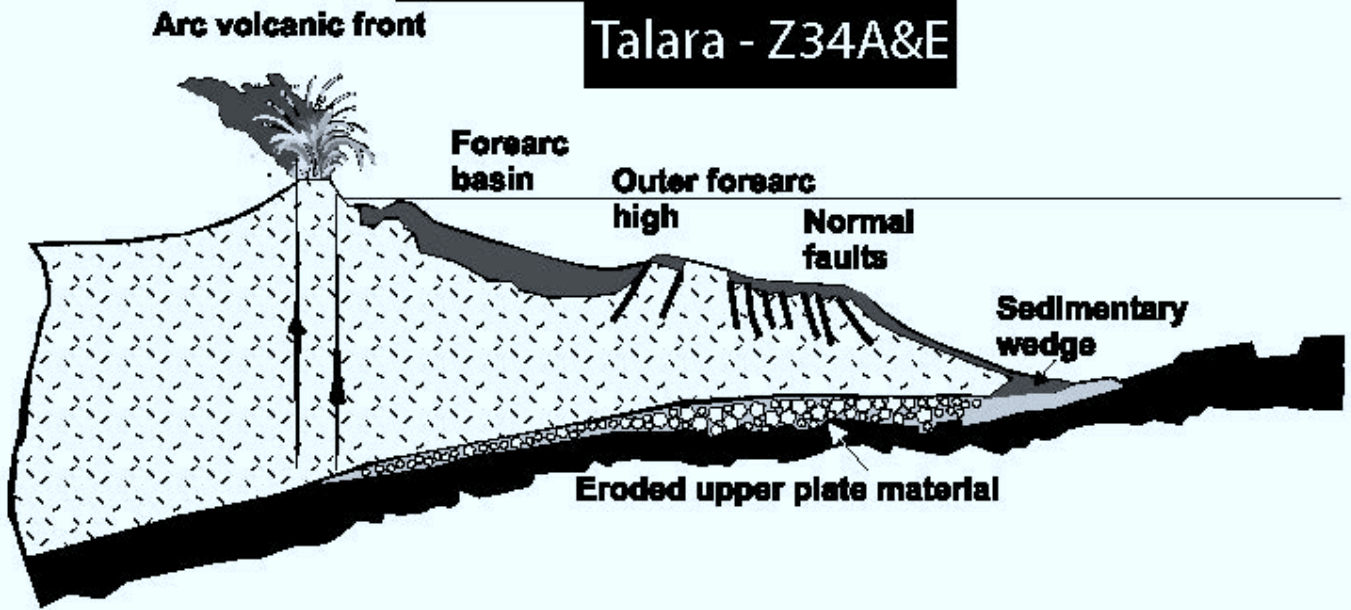
Pisco - Z33 Tumbes - Z1&38

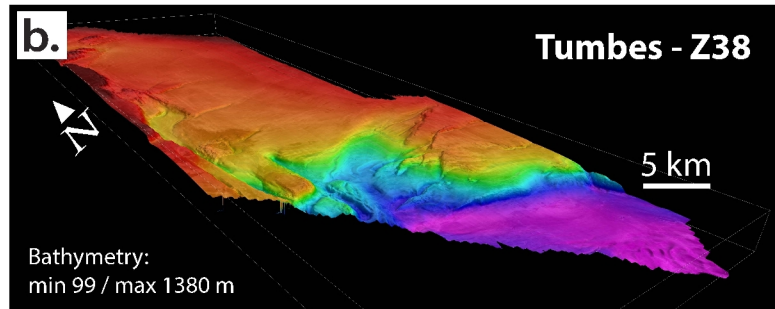
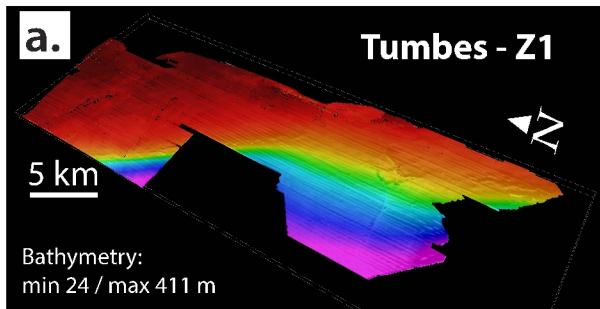


b.

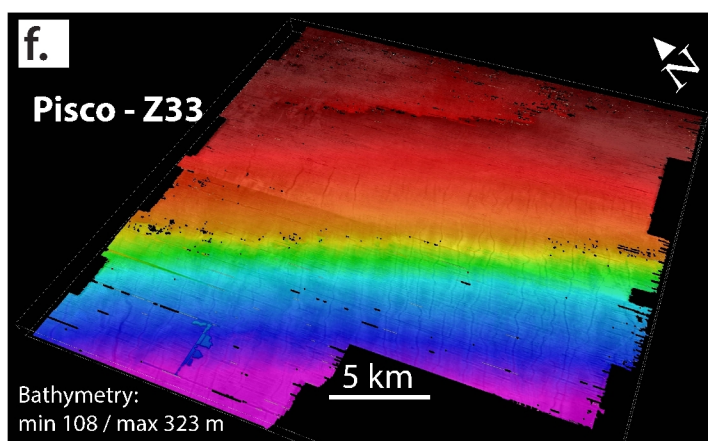
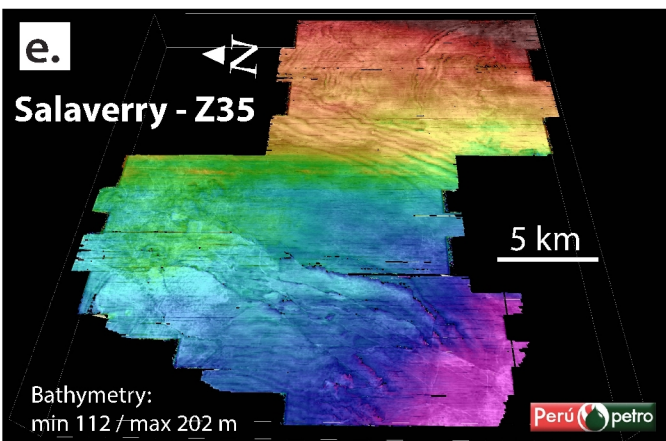
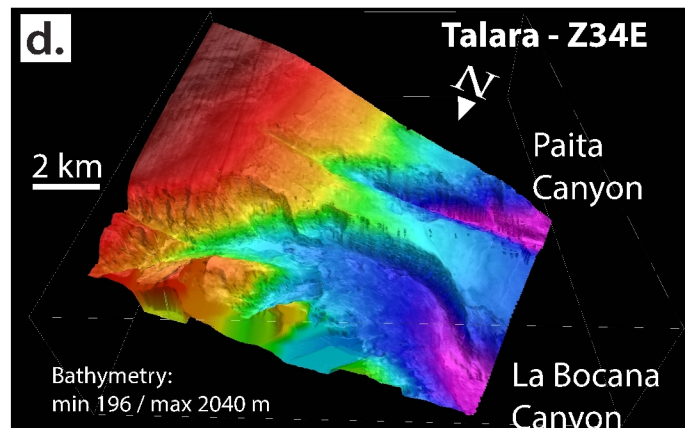
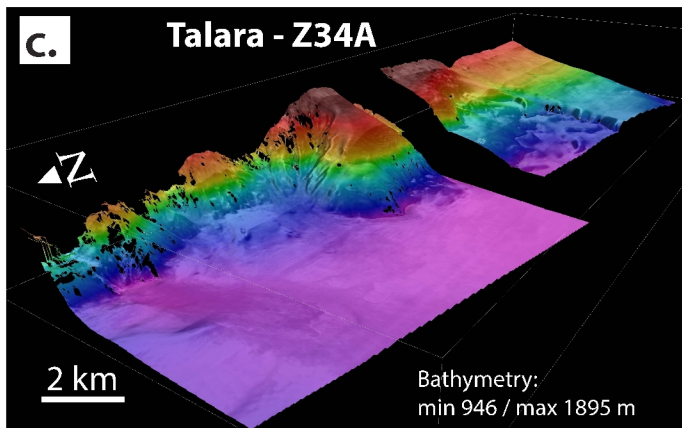
Salaverry - Z35

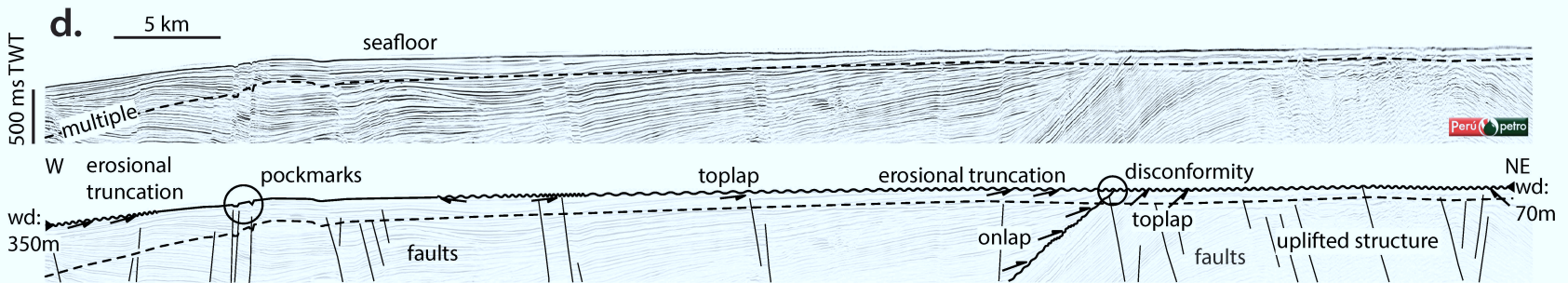
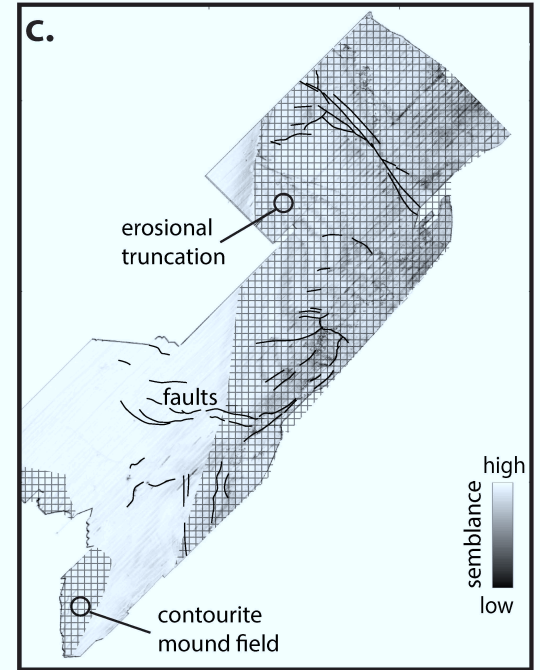
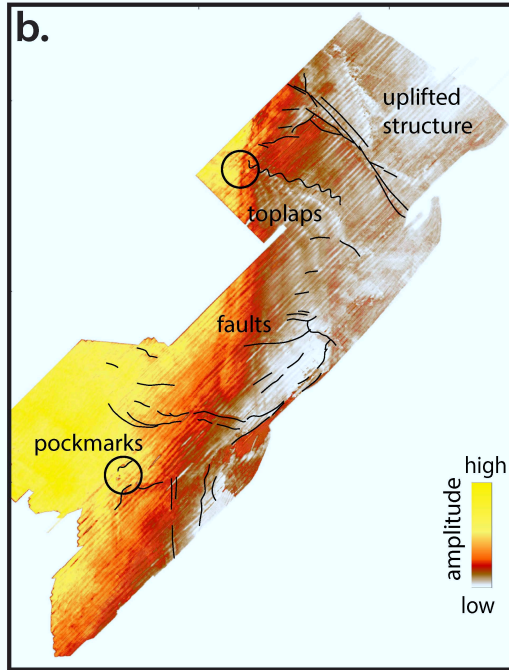
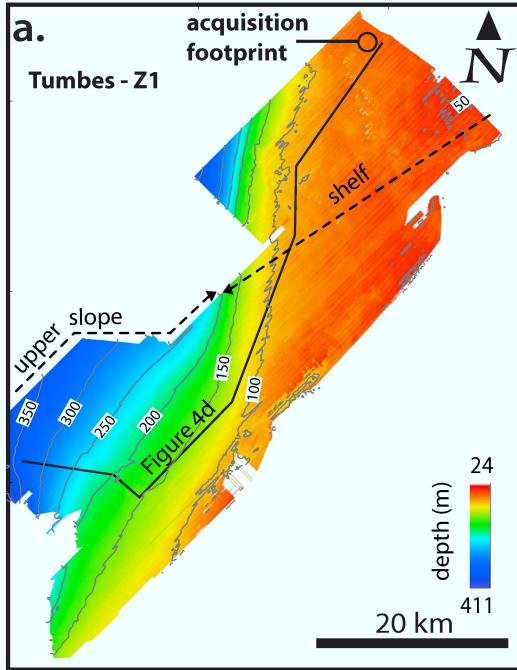
Talara - Z34A&E

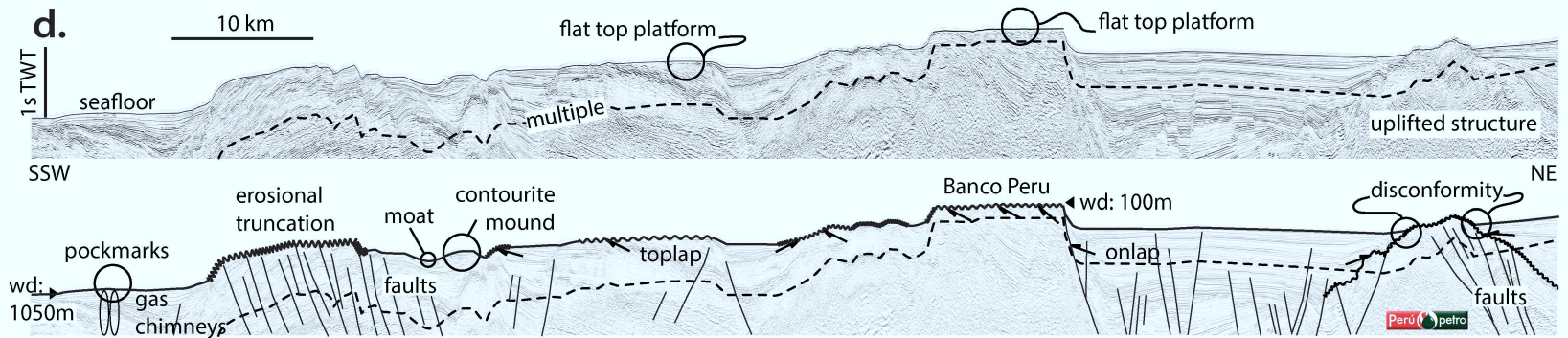
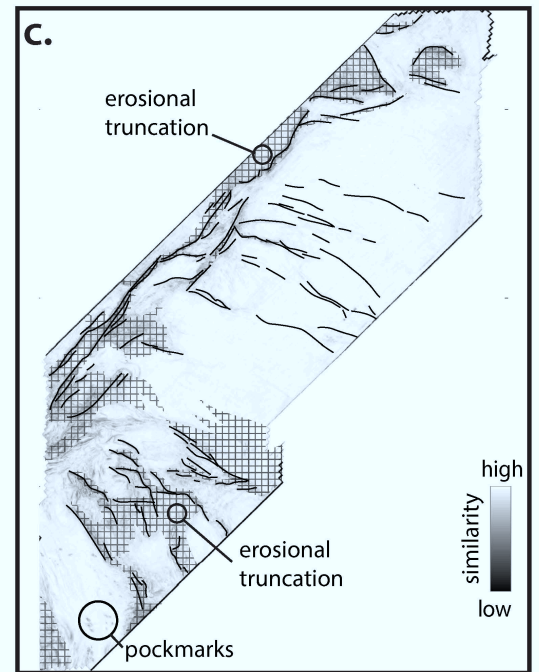
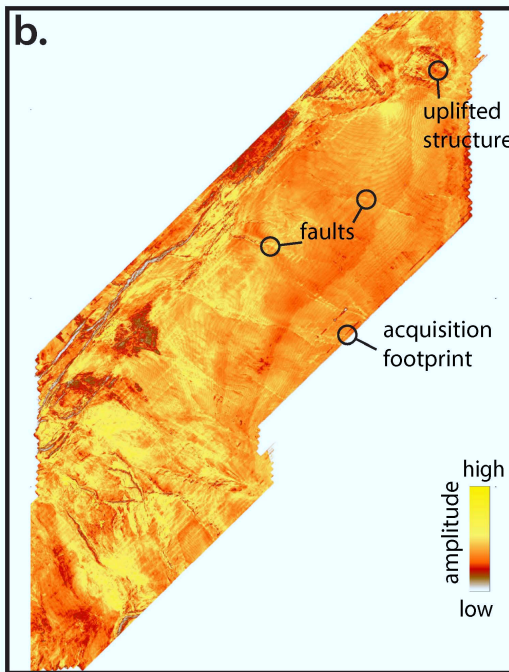
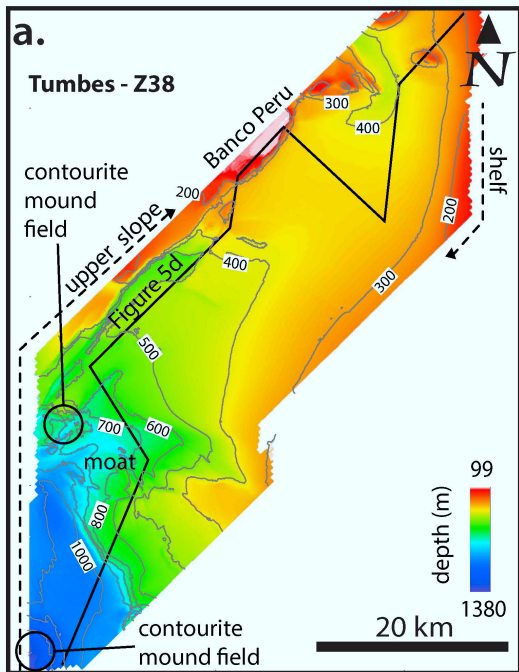


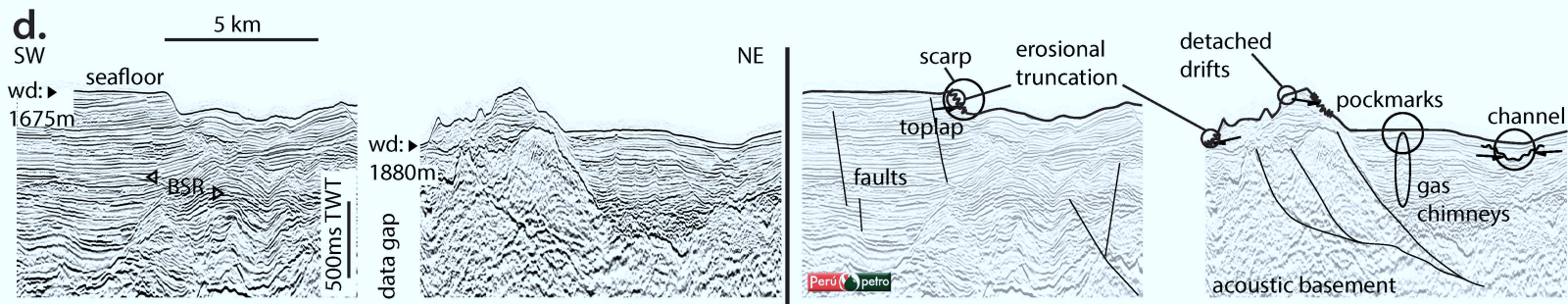
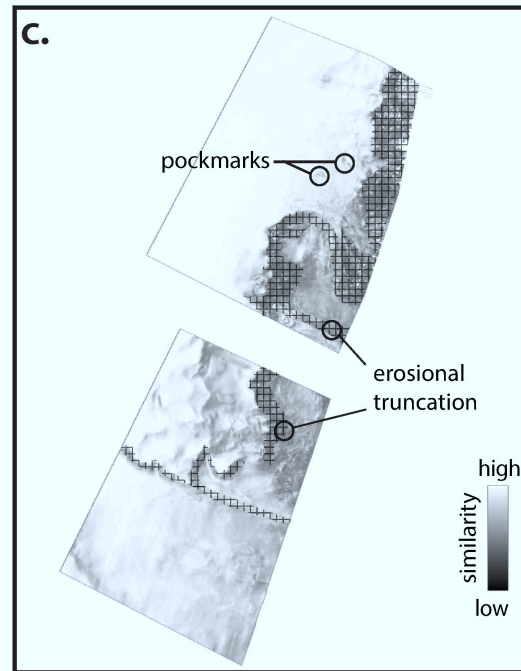
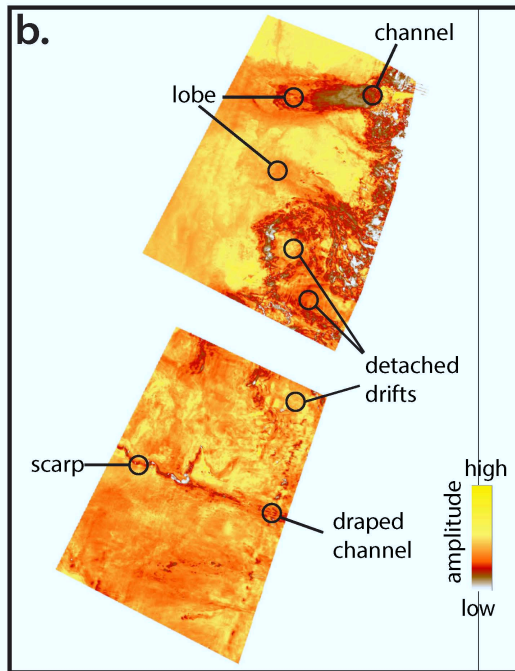
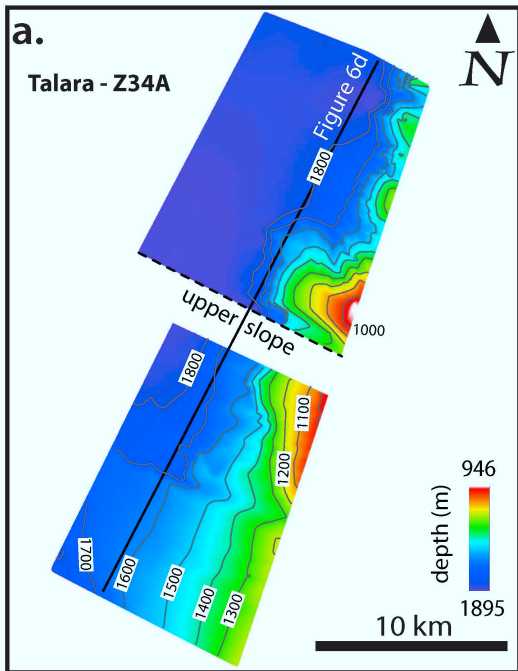


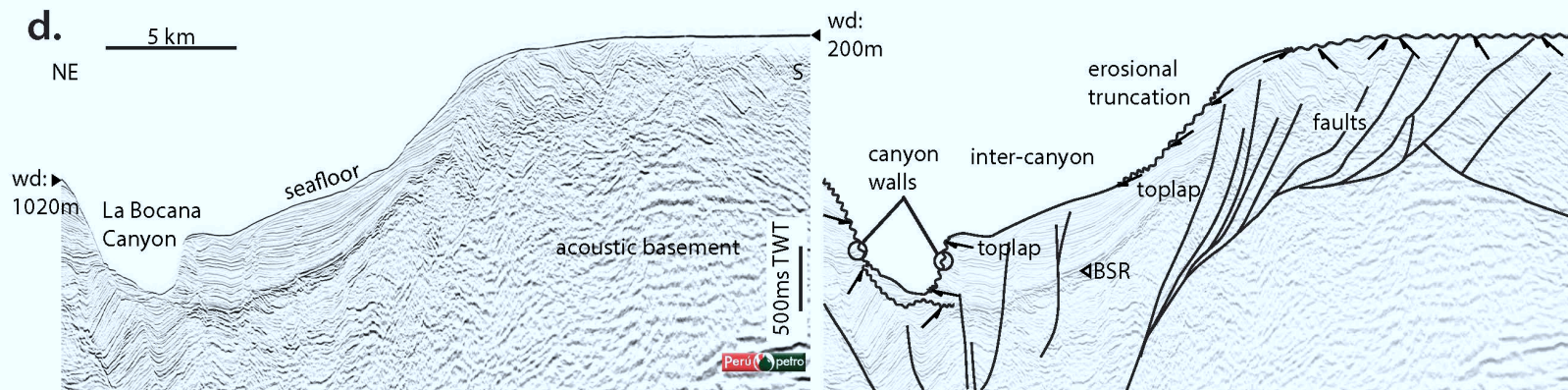
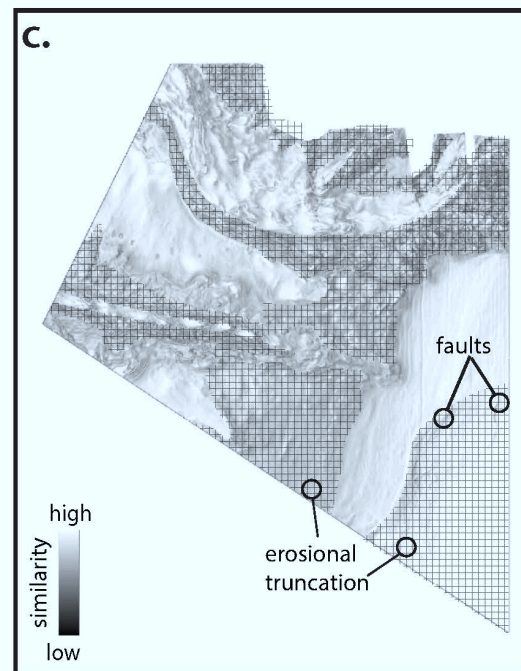
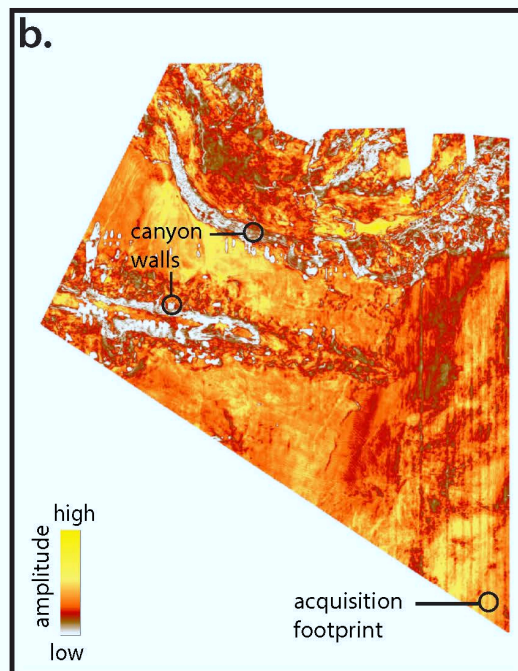
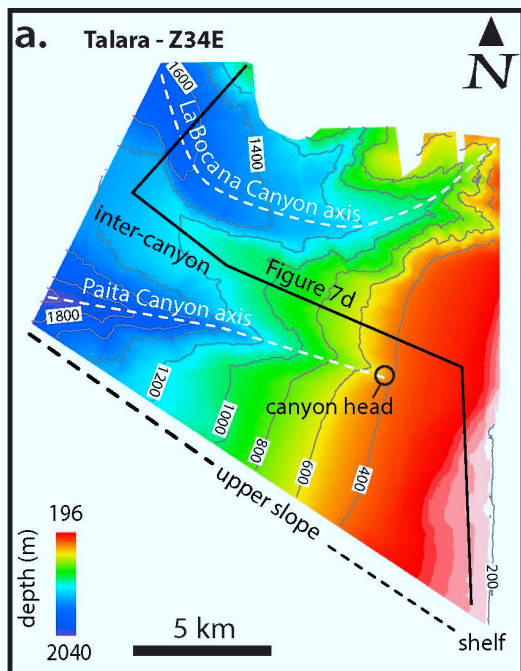
bathymetry
shallow deep

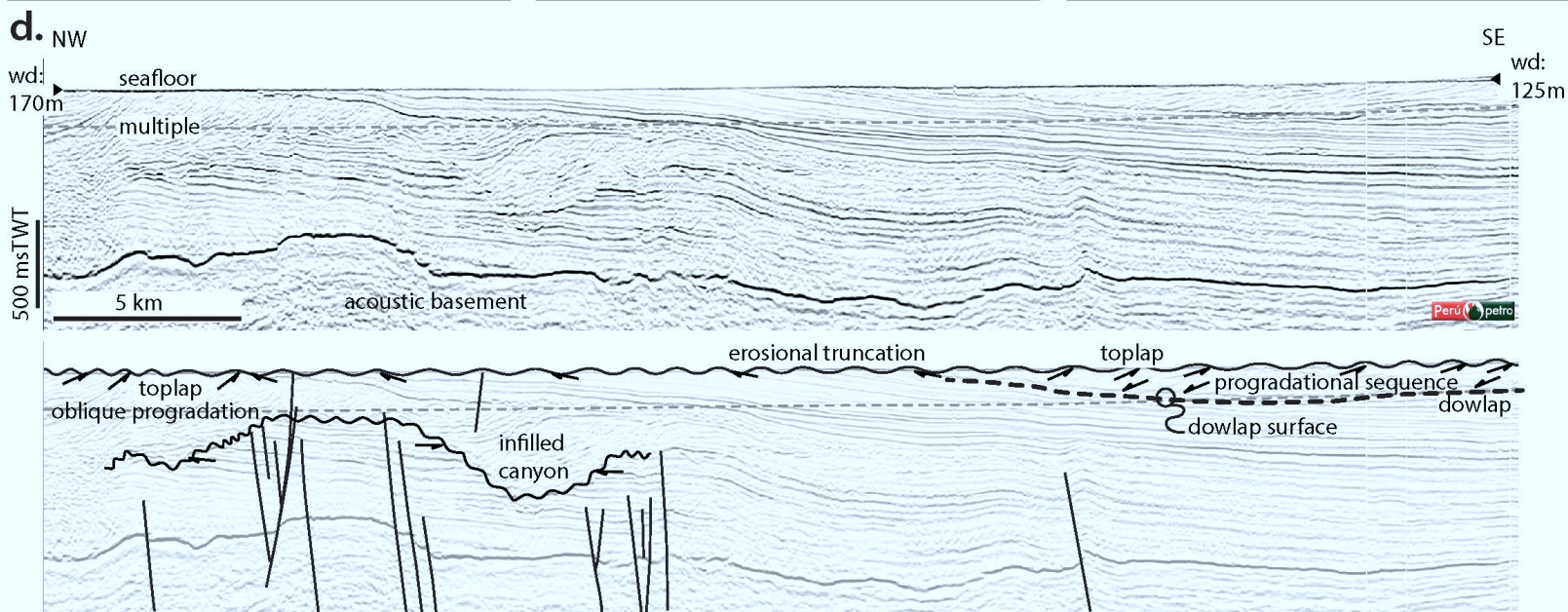
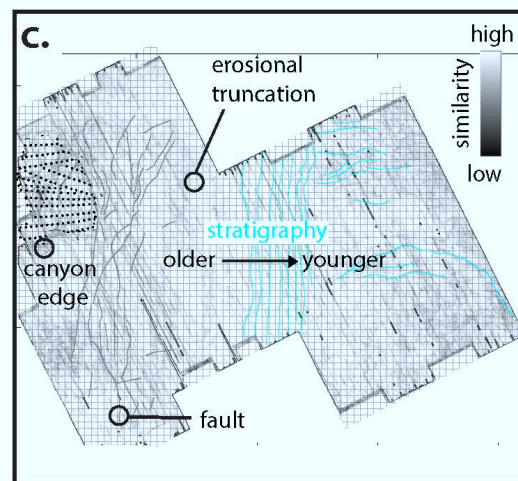
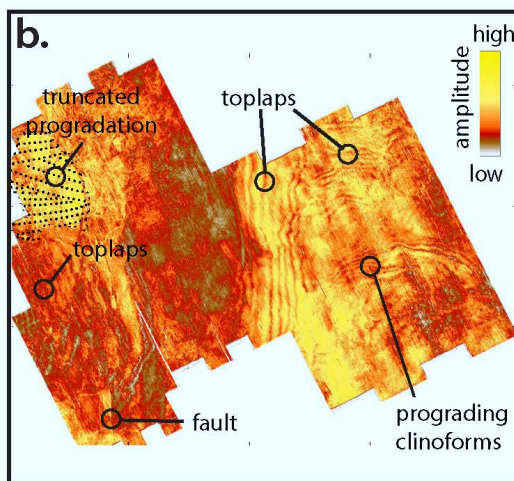
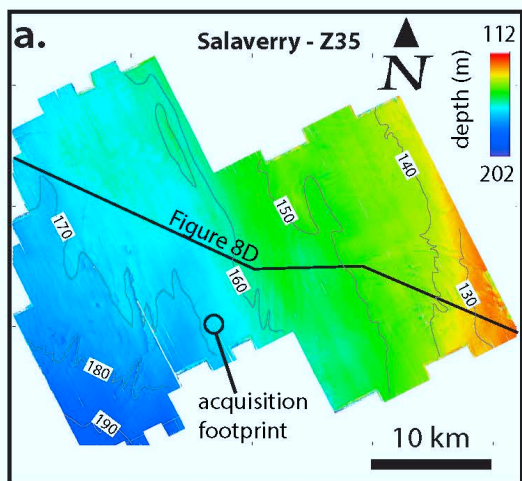


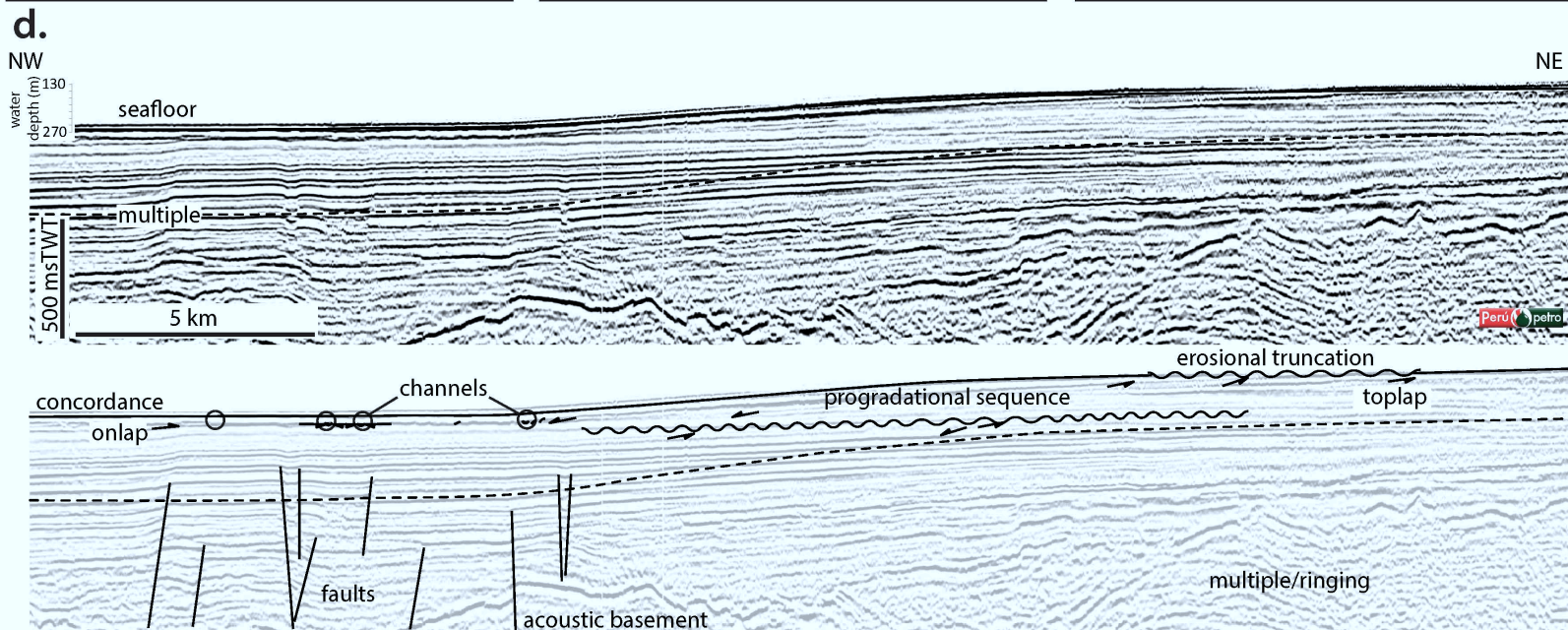
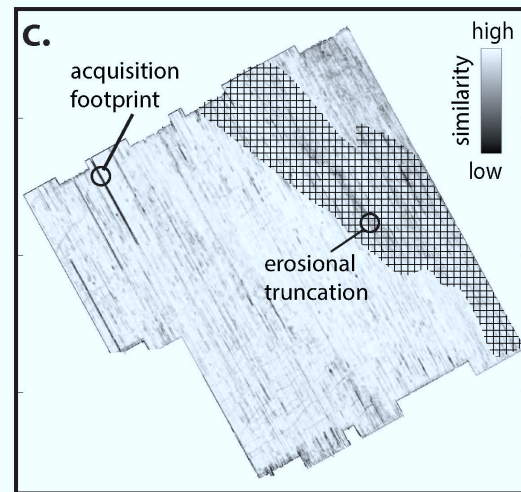
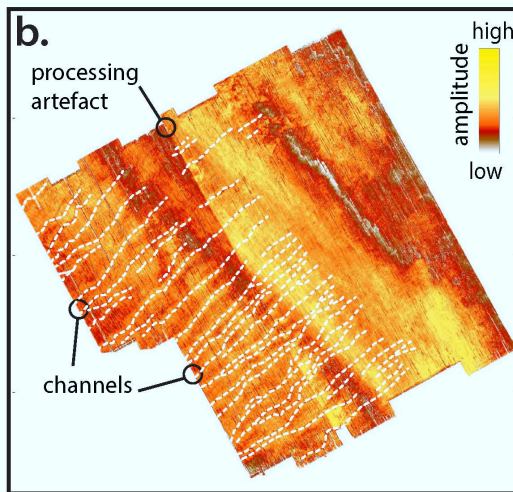
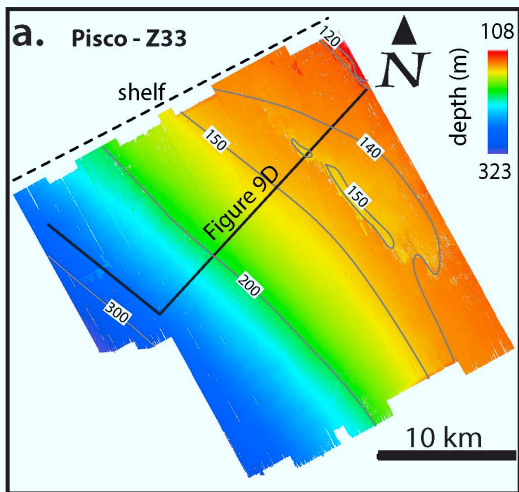


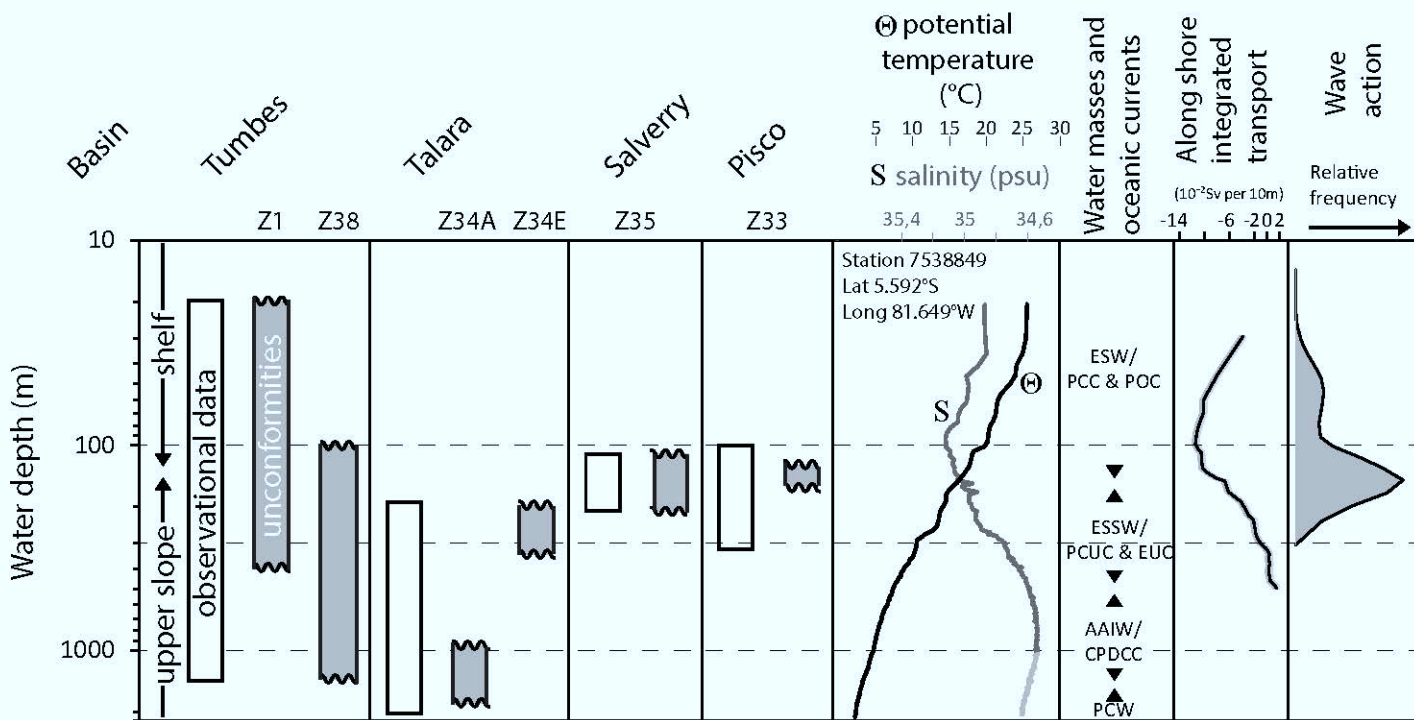












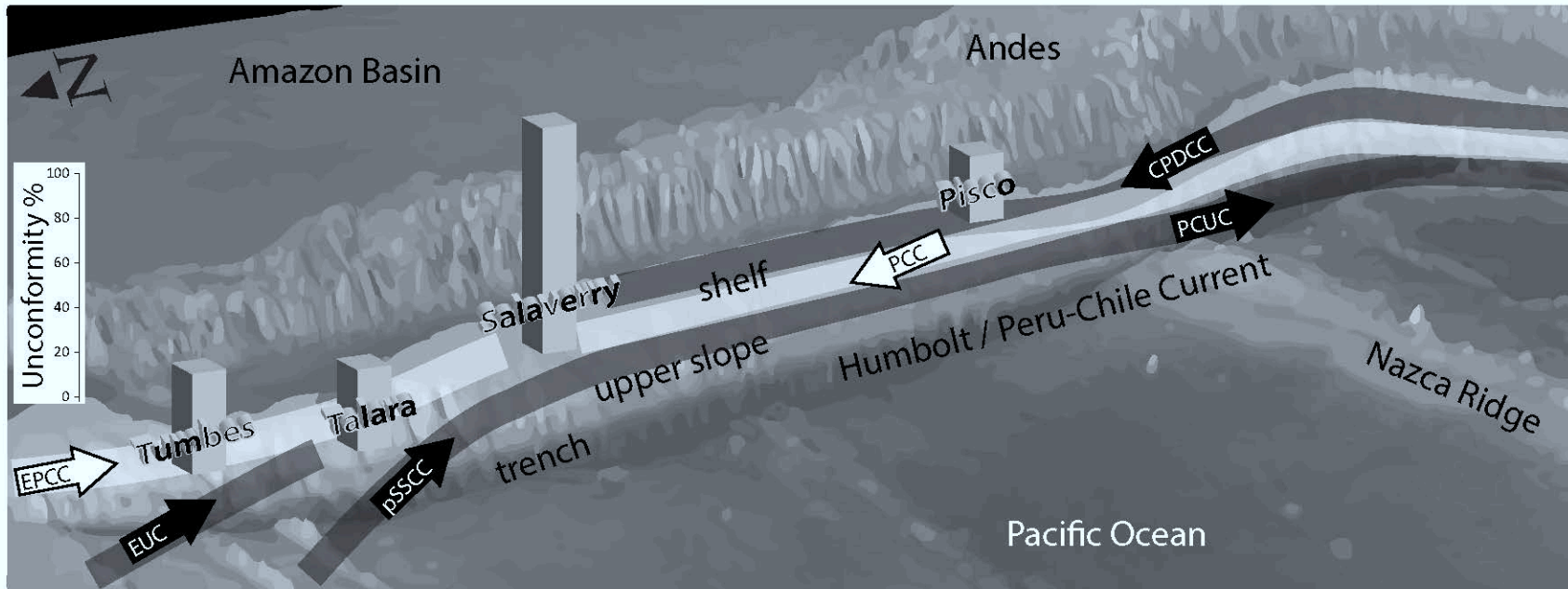


Table 1 : Geographical and morphological properties of the seafloor for the four sedimentary basins within the 3D seismic data volumes used for this study.

Sedimentary basin	Dataset / seismic cube	Latitude	Bathymetry		Survey area km ²	Peak frequency Hz	Tuning thickness - vertical resolution m	Slope mean (degree)	Domain
			min (m)	max (m)					
Tumbes	Z1	3°45'S	24	411	1300	40	10	3.6	Shelf and upper slope
	Z38	4°15'S	99	1380	1620	43	9	2.6	Shelf and upper slope
Talara	Z34A	4°20'S	946	1895	194	47	8	5.95	Upper slope
	Z34E	5°S	196	2040	215	35	11	10	Shelf and upper slope
Salaverry	Z35	8°S	112	202	880	35	11	1.75	Shelf
Pisco	Z33	12°30'S	108	323	663	32	12	1	Shelf and upper slope

Accepted Article

Table 2: Morphological and seismic properties of the various features observed within the 3D seismic data volumes used for this study, and their interpretation.

Sedimentary basin	Dataset / seismic cube	Feature/shape				Interpretation			Unconformity % (minimum/mean/maximum)
		linear	rounded	mounds	flat top high	Structural	Sedimentary	Fluid flow	
Tumbes	Z1	x	x	x		faults / uplifted structures	erosional unconformities, contourite drift,	pockmarks	26/44/68
	Z38	x	x	x	x	faults / uplifted structures	erosional unconformities, contourite drift, moat	pockmarks	
Talara	Z34A	x	x	x	x	faults	erosional unconformities, head scarp of mass wasting, contourite drift, channel, lobe	pockmarks	18/36/53
	Z34E	x	x	x		fault	erosional unconformities, canyons, contourite drift	not identified	
Salaverry	Z35	x	x		x	fault	erosional unconformities, prograding canyon infill, canyon edges	not identified	100
Pisco	Z33	x			x	not identified	erosional unconformities, channels, wave cut platform	not identified	29